



Universitat Autònoma de Barcelona

**Exoplanet potential from single-transit
detection: The CHEOPS-TESS synergy**

Master Thesis presented by:

Àlex Pagès Pérez

Supervised by:

Ignasi Ribas Canudas

September 2015

Course 2014-2015

Contents

1	Summary	3
2	Introduction	5
2.1	Exoplanet detection methods	6
2.1.1	The Transit Method	7
2.2	Transiting exoplanet detection missions	9
2.2.1	The Kepler Mission	9
2.2.2	The CHEOPS mission	11
2.2.3	The TESS Mission	12
2.3	Objectives	13
3	Methodology	14
3.1	Towards an estimation of transiting exoplanet period from a single transit	14
3.2	Exoplanet sample: selection & analysis	16
3.2.1	Obtaining the light curves	16
3.2.2	Selecting a sample to work with	17
3.2.3	Modeling planetary transits	19
3.2.4	Taking our output results	21
3.2.5	Errors taken into account and its propagation error formulas	22
4	Results and discussion	25
4.1	Systems analyzed with Short Cadence format	25
4.1.1	Kepler-89 d	26
4.1.2	Other cases	26
4.2	Systems analyzed with Long Cadence format	28
4.2.1	Kepler-18 d	30
4.2.2	Kepler-26 c	31
4.2.3	Kepler-27 b	31
4.2.4	Kepler-27 c	32
4.2.5	Kepler-31 b	33
4.2.6	Kepler-39 b	33
4.2.7	Kepler-117 b	34
4.2.8	Kepler-118 c	35
4.2.9	Kepler-149 b	35
4.2.10	Kepler-222 d	36
4.2.11	Kepler-229 c	37
4.2.12	Kepler-230 b	37

4.2.13 Kepler-238 e	38
4.2.14 Kepler-247 d	39
4.2.15 Kepler-248 c	39
4.2.16 Kepler-257 d	40
4.2.17 Kepler-281 c	41
4.3 Summary & interpretation of the results	42
5 Conclusions	51
6 References	53
7 Appendix	54

1 Summary

The interest in the exoplanetary research has been increased during the last years, thanks to the development of several transit surveys, such as the CoRoT and Kepler mission, or future surveys like CHEOPS, TESS and PLATO. Because each survey will be launched in order to accomplish an intrinsic objective, it is interesting to study if it is possible to find out synergies between those transit surveys, and develop them.

The final goal of this master thesis is to check the potential of single-transit exoplanets detection, specially, if it is possible to find out a unique solution for the planetary orbital periods without needing to detect several transits in those systems analyzed. Planetary transits are characterized by the decrease of stellar luminosity for several hours and they are repeated periodically. This study is quite relevant since some future transiting missions, such as TESS Mission, will be searching for exoplanets, covering an important fraction of all our sky during 28 days. This means that it will be expected to find many exoplanet candidates, detecting only one transit, with orbital periods longer than the period of observation. After that, the CHEOPS mission, which will be launched to stare at stars already known to host planets, will be able to recover those planetary transits detected by TESS, which are considered interesting to analyze in detail.

With the aim of testing our procedure, we first need to take the data for some exoplanets, whose orbital periods are already known, since they have been correctly determined by detecting several consecutive transits, and measuring the periodicity of those transits. After that, we apply our methodology by taking only a single transit (see section 3). We decide to take a sample of exoplanets discovered by Kepler mission, as around 1000 exoplanets have been confirmed by this transit survey, and a large catalog containing the parameters associated to each planet and its host star is available at the Kepler mission archive. Furthermore, the light curves gathered can be publicly downloaded.

After downloading these light curves containing exoplanetary transits, we selected a sample to be studied. Because deeper transits yield more precise parameters, we defined a cut-off on the transit depth. We also selected only those systems with orbital period from 14 to 40 days, as it will be explained in detail in section 3. After the selection, we used a preliminary sample of 22 systems, which is small enough to be analyzed, requiring a reasonable amount of time, and is large enough to provide our conclusions with statistical significance.

For each system studied, we selected a single transit and we modeled its corresponding light curve using JKTEBOP, a code originally developed with the aim to fit light curves of eclipsing binary systems, but later adapted to fit exoplanet transits. The model fits allowed

us to estimate the duration of the transits, as well as their shapes and depths, which are used to derive the orbital period of the system.

Finally, our periods, derived from a single transit, are compared to the real ones, previously determined by several transits, in order to check the reliability of the methodology applied. At the end, we analyze a total of 18 systems, 9 of which are properly modeled, 3 are moderately well modeled and the remaining 6 systems are fitted with poor accuracy. The estimated orbital periods agree well with the real periods in 7 of the 9 systems with good model fit, in the 3 systems whose fit reliability is moderate and only in 2 of the systems fitted with poor precision.

A part from needing precise model fits for light curves, we also concluded that it is required to know the density of the hosts of the exoplanets studied, if we want to determine a reliable orbital period applying the methodology of the single-transit.

2 Introduction

Since the dawn of time, humans have been interested in the existence of other worlds outside the Earth. After exploring the Solar System, with the Earth as the currently unique habitable planet, time has come to explore extrasolar systems in order to discover new worlds, which are known under the name of exoplanets.

The discovery of the first exoplanet in 1995 sparked the interest and research in this branch of Astrophysics and has been increasing progressively. Thanks to the formulation of several methodologies, as well as, the development of new tools, more than 1800 exoplanets have been discovered to date, two decades later. A clear example is the Kepler mission, the most successful transit survey so far, which has discovered more than 1000 exoplanets and detected more than 3000 other candidates, applying the so-called transit technique.

New transit surveys are planned for the future, such as CHEOPS and TESS, both expected to be launched in 2017. We shall also mention, the PLATO mission. It will be the successor transit survey of CHEOPS and TESS, with its launch targeted for 2024. TESS will find exoplanet candidates in bright stars of the solar neighborhood, whereas CHEOPS will, also, perform refined measurements by follow-up observations. PLATO will be focused on the detection and characterization of terrestrial exoplanets in the habitable zone and it will provide asteroseismology for the determination of the stellar parameters (masses, radii, ages). The conventional transit method consists in discovering an exoplanet after detecting several transits, which allows to directly determine the orbital period of the planet and, then estimate its orbital distance from the host star. However, some transit surveys are gathering data during short periods of time, as it will be the case of TESS, which, in most cases, will be staring at the same stellar field for around 28 days. This means that more than one transit can not being detected for systems with periods longer than 14 days.

Here is where the interest of finding out almost all planetary parameters from just a single transit arises. By discovering its orbital period we can solve questions like ‘is this planet in the habitable zone?’ and determine some of its key properties. Seager & Mallén-Ornelas (2003) discussed how to estimate planetary and stellar parameters using information from a single transit, including the orbital period, which can be estimated from an analytical solution that depends on the transit parameters and the stellar density. These transit parameters are the transit duration, the flat transit duration (the period of time when the planet is seen completely inside the stellar disk) and the transit depth.

In this section, we will introduce some exoplanet discovery techniques, entering into more details about transit method (subsection 2.1). In subsection 2.2, we will do an overview about the transit surveys in which the methodology and results of this master thesis are based

(Kepler, CHEOPS & TESS).

2.1 Exoplanet detection methods

Here we present several techniques developed so far, to detect extrasolar planets. These are not all possible detection methods, but we briefly discuss those that have been produced at least one successful detection¹² (Fischer et al., 2014).

1 - Radial velocity method: This technique is based on the Doppler Effect. As a response of the gravitational influence caused by a near planet, central star describes a small reflex orbit, moving away and towards the Earth, periodically. These movements cause redshift and blueshift on the stellar spectral lines, respectively. Radial velocity method allows to determine the eccentricity of the orbit and put a minimum planetary mass constraint, as its calculated value depends on the orbital inclination with respect to the observer. This was the most successful method until the launch of Kepler Mission.

2 - Transit photometry method: This has been the most successful technique during the last years and can be applied to detect with certain facility not only giant planets, but also Earth-like exoplanets. It is based on the stellar photometry measure, such that if the flux coming from any star slightly decreases for a certain period of time, this means that a body has passed between the star and the observer. Applying this technique it is possible to determine the radius of the planet, so it is usually well complemented with the radial velocity technique. The main disadvantage of this method is that requires the orbital plane to be almost perfectly aligned to the observer. The Kepler Mission and future searching surveys like CHEOPS, TESS and PLATO are based on this method. A more exhaustive explanation will be provided later.

3 - Direct imaging: In some cases it is possible to detect planets by seeing them directly, if observed in infrared light. Because planets are much fainter than stars, this method is only applicable for giant (usually larger than Jupiter) and very hot planets that orbit small stars. These conditions occur when the planetary systems are young, so planetary gases are still hot, as a result of its recent formation stage, and contracting.

4 - Microlensing method: Microlensing occurs when two stars, situated at different distances, are nearly aligned to an observer, being the nearer star the lens star and the farther star, the source star, whose image is deformed and deflected from its true position by the gravitational field of the lens star. If the lens star contains an orbiting planet and this passes

¹<http://www.smithsonianmag.com/science-nature/how-do-astronomers-actually-find-exoplanets-180950105/?no-ist>

²https://en.wikipedia.org/wiki/Methods_of_detecting_exoplanets

in front of the source’s image, then the planet adds a new deformation to the image, causing a peculiar effect on the light curve of the microlensing source star. This technique can be applied to systems situated large distances away from us, but it cannot be applied twice for the same system.

5 - Timing variations: Orbiting planets can alter the duration of periodic phenomena on stars or other planets, orbiting them. This method is based on the observation of these phenomena and measure their duration as it changes with time. This methodology can be applied to the pulsar timing of a neutron or a variable star, the deviation of the periodicity of a transit and the change on the transit duration.

Most of the detection methods explained above are not based on direct observations (only imaging is a direct method), but they are based on the study of the stellar physics or phenomena, which can be related to the presence of other bodies that are orbiting a star, so they are indirect methods. The radial velocity and the transit methods are, by far, the most successful methods and both are well complemented with each other.

Since in this project we will address the transit photometry method and we will base our final conclusions on the possibility of synergies between the CHEOPS and TESS missions, both based on the transit method, we are explaining it in detail next.

2.1.1 The Transit Method

A transit occurs when a small object passes between a larger celestial body and an observer. When the small object that crosses in front of a star is a planet, we call this phenomenon ‘planetary transit’. These transits are detected by measuring the flux emitted by a distant star that reaches an observer telescope, as the flux is reduced during transit time (see Figure 2.1). Observing that the same transit is repeated periodically, the orbital period of the planet can be directly obtained.

Because the luminosity measured by the observer depends on the intrinsic size of the source and planets do not produce light on their own, it is derived that the ratio between planetary radius (R_p) and stellar radius (R_*) are related to the transit depth by:

$$\Delta F = \frac{F_{no\ transit} - F_{transit}}{F_{no\ transit}} = \frac{R_p}{R_*} \quad (2.1)$$

This is the most successful exoplanet detection method nowadays, thanks to which several types of planets have been found, including terrestrial planets located in the habitable zone of their host star. It also has the advantage that is possible to obtain large samples of candidate exoplanets by staring at many stars at the same time. Actually, the Kepler Mission has announced more than 3000 possible candidates. We understand by terrestrial planets, those

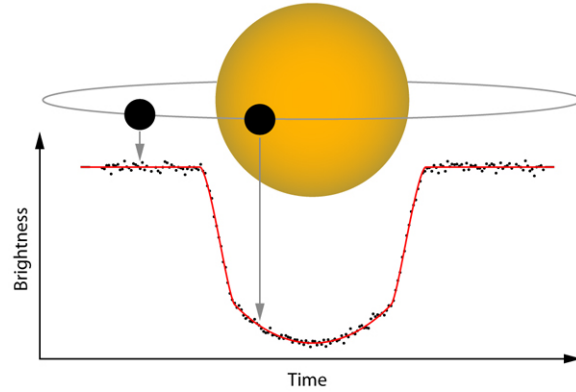


Figure 2.1: Representation of a planetary transit in front of a star and its light curve.

between half and twice the Earth's size, and the habitable zone of a star is defined as the region where the equilibrium temperature allows the presence of liquid water. The distance of the habitable zone to the star depends on the stellar type.

In contrast, this technique presents the drawback that the orbital plane needs to be almost perfectly orientated edge-on to the observer, otherwise the planetary transit would not happen. The transit occurrence chance is directly proportional to the size of the host star and inversely proportional to the distance to the star. This can be shown defining the impact parameter, b . This parameter is normalized according to the stellar latitude that the planet crosses during the transit. In this way $b = 0$ means that the planet transits the star across its equator, whereas $b = 1$ means that the planet passes only through a pole of the star. Then, assuming the approximation that the planet is a dimensionless point, transits would not be possible for impact parameters larger than the unity.

$$b = \frac{a}{R_*} \cos i \quad (2.2)$$

Here, a is the semi-major orbital axis and i is the angular inclination of the normal axis of orbital plane with respect to the line of sight. The angle is close to 90° when transits are detected.

A transit is basically described by its depth (Equation 2.1) and its shape, which is characterized by how long the planet is ingressing into and/or egressing out of the transit, and how long the planet is completely inside the transit (Figures 2.1 & 2.2).

In the ideal case, light curves should be flat when the planets are completely inside the transit, but this does not happen because of the stellar limb darkening (LD). LD occurs because the edge of a star is less luminous than the center, as viewed by an observer. This is

reflected on the light curve, in the way that it is not flat in the central region, but there is a minimum of flux at the center of the transit. The transit shape also depends on the impact parameter, as the curve follows a "U" shape when the impact parameter is low, while it acquires a "V" shape when the impact parameter is nearly 1, as shown in Figure 2.2. This is explained as the higher is the impact parameter, the smaller is the fraction of the flat transit duration.

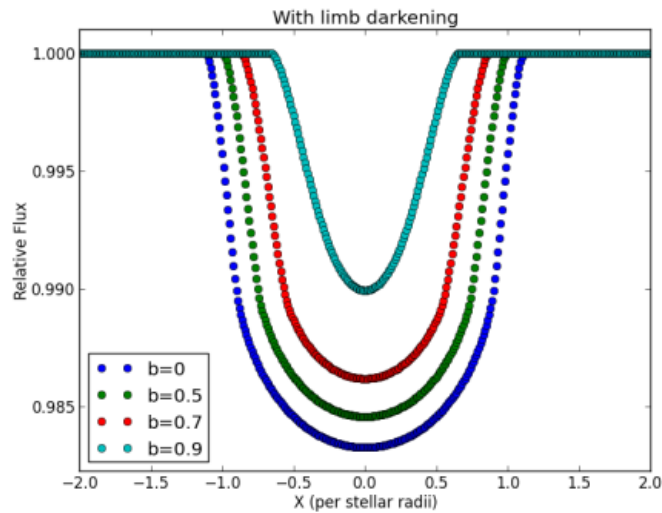


Figure 2.2: Light curve change during a transit for different impact parameter and considering stellar limb darkening.

2.2 Transiting exoplanet detection missions

2.2.1 The Kepler Mission

The Kepler mission has been one of the most successful exoplanet search missions so far and it was based on the transiting method. The increasing interest in discovering new worlds able to host life, during the last decades, inspired the researchers to carry out this space mission. It was launched in March 2009, with the proposal of being storing flux measurements, at least, for four years long. Due to the success of the transit survey, the duration of the mission was extended. However, the mission was finally over in May 2013, due to an internal failure within one of their reaction wheels ¹. Fortunately, the Kepler team succeed in keeping the spacecraft working, making possible to continue Kepler's discoveries with the K2 mission, with the limitation of being able to scan the regions near the ecliptic plane ².

¹<http://kepler.nasa.gov/news/nasakeplernews/index.cfm?FuseAction=ShowNews&NewsID=272>

²<http://keplerscience.arc.nasa.gov/K2/>

The Kepler's gathering light curves time is divided in 17 periods of around 90 days, defined as quarters (Q). The data gathered by the Kepler Telescope are still being analyzed nowadays, having found nearly 4000 candidates, and around 1000 of them had been confirmed as exoplanets as of April 2015.

Before the Kepler Mission started operations, known exoplanets were classified, basically into three categories: gas giants, ice giants and hot-super-Earths located close to their host stars. Kepler found other types of exoplanets. It found not only gas giants or close-in hot exoplanets, but also rocky planets located relatively far from their stars. Its discoveries also include several Earth-like planets (those with half to twice the terrestrial size), accomplishing the main goal of the mission, which was to discover terrestrial planets in the habitable zone of a wide variety of stars, including Sun-like stars (this explains as a necessity the long duration of the mission).

A clear example is the recent discovery of the system Kepler-452b, confirmed in July 2015 (Jenkins et al., 2015). It is considered the discovered exoplanet, up to date, which most resembles our Earth, as it has a terrestrial size, is located in the habitable zone of a Sun-like star and is supposed to gather the necessary conditions to harbor life.

Because Kepler analyzed the flux of a great number of stars (around 100000 stars located towards the Orion Arm, in the Milky Way), Kepler planetary discoveries can be used to perform a statistical study about the abundances of exoplanets, such as terrestrial planets in the habitable zone, in the whole Galaxy. A study performed by Burke et al. (2015) reveals that the occurrence rate for one year orbital period terrestrial planet and for the Kepler G target sample is $\zeta_{1,0} = 0.1$, with an allowed range of $0.01 \leq \zeta_{1,0} \leq 2$. Another study (Fressin et al. 2013) shows that $16.5 \pm 3.6\%$ of main-sequence FGK stars have at least one planet between 0.8 and 1.25 Earth radii, with orbital periods up to 85 days.

The Kepler project has provided ground-breaking new insights into the population of exoplanets in our Galaxy. Among the discoveries made using data from Kepler is the fact that the most common members of the exoplanet family are Earths and Super-Earths. However, the majority of exoplanets found by Kepler orbit faraway, faint stars. This, combined with the relatively small size of Earths and Super-Earths, means that there is currently a dearth of such planets that can be characterized with follow-up observations. These types of exoplanets are expected to be found by the next transit survey generation (CHEOPS, TESS, PLATO) and then there will be characterization by performing follow-up observations (JWST, ARIEL).

2.2.2 The CHEOPS mission

CHEOPS (CHAracterising ExOPlanet Satellite) is an ESA S-class mission and the first one dedicated to searching for exoplanetary transits by performing ultra-high precision photometry on bright stars already known to host planets. Its launch is planned for 2017.

Knowing where to look and what time to observe makes CHEOPS the most efficient instrument to search for shallow transits and to determine accurate planetary radii in the super-Earth to Neptune mass range ¹.

The main science goals of the CHEOPS mission will be to measure the density of exoplanets with sizes/masses in the super-Earth - Neptune range orbiting bright stars (V -magnitude ≤ 12), and to select the optimal targets for future deeper characterization studies of exoplanets in these mass and size ranges.

In particular, CHEOPS will ²:

- Perform first-step characterizations of super-Earths, by measuring the radii and densities in a planetary mass range for which only few data exist and to a precision never achieved before, and by identifying planets with significant atmospheres as a function of their masses, distances to their stars, and stellar parameters.

- Obtain new insights into the physics and formation processes of Neptune-like planets by measuring accurate radii and densities for these planets, deriving minimum values for their gas mass fractions, and inferring possible evolution paths.

- Provide suitable targets for future ground-based (e.g., E-ELT) and space-based (e.g., JWST, ARIEL) instruments with spectroscopic capabilities. With well-determined radii and masses, CHEOPS planets will constitute the best sample of targets for such future studies.

- Probe the atmospheres of known 'hot-Jupiters' in order to study the physical mechanisms and efficiency of the energy transport from the day side to the night side of the planet.

As a minimum requirement, the total number of photoelectrons measured by the CHEOPS detector in the visible range (from 400 to 1100 nm) should correspond to source photon noise of 150 ppm/min for a $V = 9$ magnitude star. CHEOPS should be able to cover at least 50% of the whole sky for a minimum total duration of 50 days of observation per year and per target. The observation may be interrupted up to 50% (goal would be 20%) of the satellite orbital duration. This requirement is related to the science goal of detecting shallow transit ³.

¹<http://cheops.unibe.ch/science/scientific-objectives/>

²<http://sci.esa.int/cheops/54031-objectives/>

³<http://cheops.unibe.ch/science/measurement-requirements/>

2.2.3 The TESS Mission

The Transiting Exoplanet Survey Satellite (TESS) is a NASA Explorer-class planet finder. TESS will identify planets ranging from Earth-sized to gas giants, orbiting a wide range of stellar types and orbital distances. Its principal goal is to detect small planets orbiting bright host stars in the solar neighborhood, so that detailed characterizations of the planets and their atmospheres can be performed (Ricker et al. 2014).

TESS will monitor the brightnesses of more than 500000 stars during a two-year mission, searching for planetary transits, and is expected to catalog more than 3000 transiting exoplanet candidates ¹. TESS will also detect small rock and ice planets orbiting a diverse range of stellar types and covering a wide span of orbital periods, including rocky worlds in the habitable zones of their host stars. Numerical simulations, performed by Sullivan et al. (2015) show that approximately 1700 will be found by TESS and around 550 of which will have a smaller size than twice the Earth radius. It is also expected to find out 1100 planets between 2-4 R_{\oplus} and less than 100 planets larger than 4 R_{\oplus} .

The TESS scanning strategy will cover almost all the sky with 26 sectors with $96^{\circ} \times 24^{\circ}$ field of view. The observation time will be 27.4 days per each sector and the mission will last for a total of 2 years (one for each hemisphere). The regions located near from the celestial poles will be observed continuously for almost a year, whereas around 3 quarters of the sky will be observed for at least 27 days (Figure 2.3).

TESS will observe from a unique High Earth Orbit. This novel orbital system is characterized by providing unobstructed view for continuous light curves. TESS will describe two orbits of 13.7 days per sector, being in stable 2:1 resonance with Moon's orbit (Ricker et al. 2014).

TESS stars will be 30-100 times brighter than those surveyed by the Kepler satellite, so TESS planets should be far easier to characterize with follow-up observations. TESS will provide a catalog of the nearest and brightest stars hosting transiting exoplanets for further more detailed characterization with other large ground-based and space-based telescopes of the future. This project will be in good synergy, for example, with CHEOPS, which will be able to perform follow-up observations, providing refined measurements of the planet masses, sizes, densities, and atmospheric properties.

¹<http://tess.gsfc.nasa.gov/>

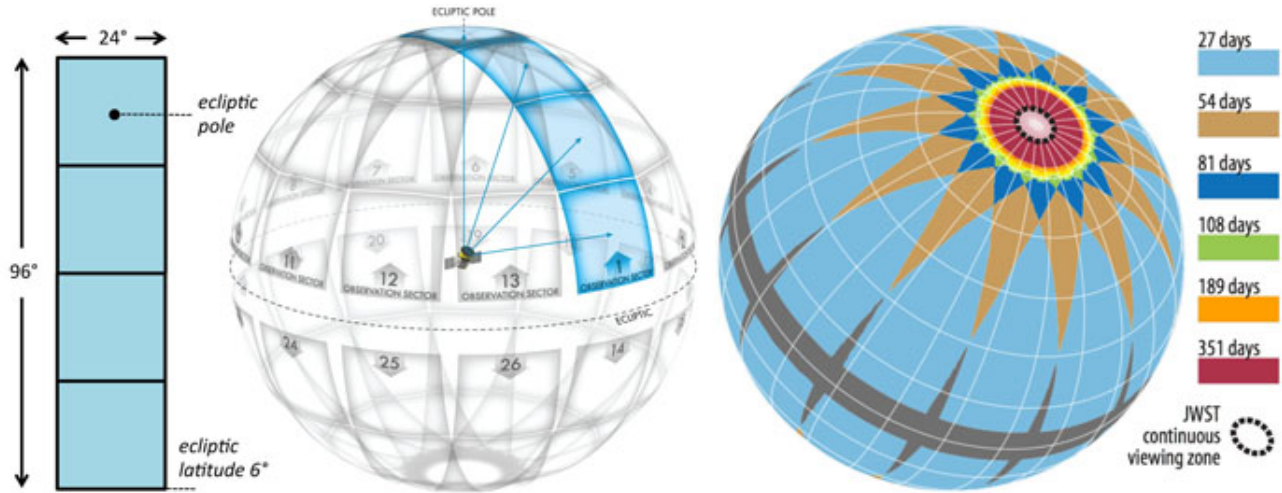


Figure 2.3: Instantaneous field of view combined with the four TESS cameras (left), division of the celestial sphere into the different 26 observation sectors (middle) and duration of observations on the celestial sphere taking into account the overlap between sectors (right).

2.3 Objectives

The main aim of this master thesis is to study whether the orbital period of a planet can be properly determined by having data from just one transit. To do that, we test some equations based on the estimation of the orbital planetary period from the observables of a light curve. They will be applied to a sample of light curves containing confirmed exoplanets, whose parameters have already been determined and their orbital periods are well known since they had been previously measured from the periodicity of several consecutive transits. In order to be able to apply our methodology, we have to derive both the full transit duration and the transit ingress/egress duration by taking a single transit from the light curves.

Once we have performed our study, we will be able to judge, according to our results and uncertainties, if the future exoplanet candidates that will be detected by TESS through a single-transit event, will be worth studying by follow-up observations with CHEOPS.

3 Methodology

3.1 Towards an estimation of transiting exoplanet period from a single transit

It has been mentioned that we need to detect at least two equal transits to directly determine the orbital period of an exoplanet. However, in many cases just one transit is detected throughout the whole observation time, due to the fact that observation time is not long enough for an exoplanet that orbits far from its host star.

Because of that, it is interesting to make some assumptions, in order to reach to some analytical expressions that allow us to estimate the orbital periods of the candidate exoplanets from the observables measured from their transits (Seager & Mallén-Ornelas 2003). These observables are the transit depth, transit duration and the flat transit duration. A transit is divided into different sections: ingress duration ranges from contacts 1 to 2 (the planet is entering the stellar disk), flat transit duration, from contacts 2 to 3 (the planet is completely inside the stellar disk) & egress duration, from contacts 3 to 4 (the planet is leaving the disk). This is shown in Figure 3.1.

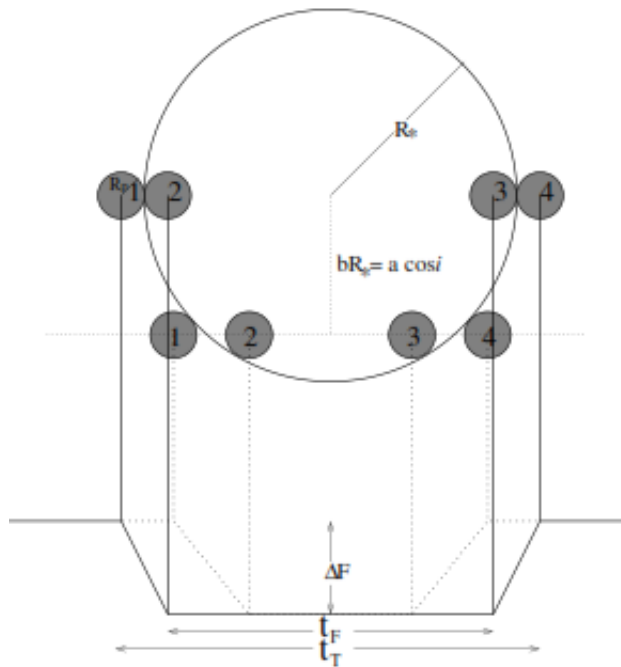


Figure 3.1: Representation of the evolution of a planetary transit in front of its host star.

t_T is the duration of the full transit from contacts 1 to 4, whereas t_F is the duration of the

flat transit from contacts 2 to 3.

The transit shape, described by the ratio between flat transit time and the total transit time, is given by the equation (Seager & Mallén-Ornelas 2003):

$$\frac{t_F}{t_T} = \frac{\arcsin \left(\frac{R_*}{a} \left[\frac{\left(1 - \frac{R_p}{R_*}\right)^2 - \left(\frac{a}{R_*} \cos i\right)^2}{1 - \cos^2 i} \right]^{\frac{1}{2}} \right)}{\arcsin \left(\frac{R_*}{a} \left[\frac{\left(1 + \frac{R_p}{R_*}\right)^2 - \left(\frac{a}{R_*} \cos i\right)^2}{1 - \cos^2 i} \right]^{\frac{1}{2}} \right)} \quad (3.1)$$

And the total transit duration is:

$$t_T = \frac{P}{\pi} \arcsin \left(\frac{R_*}{a} \left[\frac{\left(1 + \frac{R_p}{R_*}\right)^2 - \left(\frac{a}{R_*} \cos i\right)^2}{1 - \cos^2 i} \right]^{\frac{1}{2}} \right) \quad (3.2)$$

These equations are highly simplified if we consider the approximations $\frac{t_T \pi}{P} \ll 1$ and $\cos i \ll 1$. The second approximation is almost always good, since the orbital plane needs to be nearly perpendicular to observe the planetary transit. The first approximation uses that $\sin x \approx x \approx \arcsin x$ when x is small. We have to consider that the transit duration is inversely proportional to the velocity of the planet, so then by the virial theorem we have:

$$t_T \propto \frac{1}{V} \propto \frac{\sqrt{a}}{\sqrt{M}} \quad (3.3)$$

And from Kepler's Third Law we have $P \propto a^{3/2} / M^{1/2}$, which results into:

$$\frac{t_T}{P} \propto \frac{\sqrt{a}}{\sqrt{a^3}} \propto \frac{1}{a} \propto \frac{1}{P^{2/3}} \quad (3.4)$$

This means that the approximation is better when period is longer.

Under these approximations and coming back to Seager & Mallén-Ornelas (2003), Equations (3.1) & (3.2) can be simplified as:

$$\left(\frac{t_F}{t_T} \right)^2 = \frac{(1 - \sqrt{\Delta F})^2 - b^2}{(1 + \sqrt{\Delta F})^2 - b^2} \quad (3.5)$$

And

$$t_T = \frac{PR_*}{\pi a} \sqrt{(1 + \sqrt{\Delta F})^2 - b^2} \quad (3.6)$$

Where b is the impact parameter (Figure 3.1), which is dimensionless and it is normalized to the stellar radius (Equation 2.2). From Equation (3.5), b can be expressed as a function of light curve observables (Seager & Mallén-Ornelas 2003):

$$b^2 = \frac{(1 - \sqrt{\Delta F})^2 - \left(\frac{t_F}{t_T}\right)^2 (1 - \sqrt{\Delta F})^2}{1 - \left(\frac{t_F}{t_T}\right)^2} \quad (3.7)$$

Then substituting Equation (3.7) in (3.6) and considering again the approximation $\frac{t_T \pi}{P} \ll 1$ and also $\sqrt{\Delta F} \ll 1$ we reach the expression:

$$\frac{a}{R_*} \approx \frac{2P}{\pi} \frac{(\Delta F)^{1/4}}{(t_T^2 - t_F^2)^{1/2}} \quad (3.8)$$

And finally, combining equation (3.8) with Kepler's Third Law, we obtain:

$$\frac{M_*}{R_*^3} = \frac{M_*}{a^3} \frac{a^3}{R_*^3} \approx \frac{4\pi^2}{GP^2} \frac{8P^3}{\pi^3} \frac{\Delta F^{3/4}}{(t_T^2 - t_F^2)^{3/2}} \Rightarrow \boxed{P \approx \frac{G\pi}{32} \frac{(t_T^2 - t_F^2)^{3/2}}{\Delta F^{3/4}} \frac{M_*}{R_*^3}} \quad (3.9)$$

This way, the orbital period of an exoplanet can be estimated from the observables given by a single transit. It is also derived, from the last term, that the period is directly proportional to the stellar density, and this term can be approximately derived from the stellar characteristics.

3.2 Exoplanet sample: selection & analysis

Here, the process followed to obtain the data and select a sample to be studied is explained, as well as, the procedure to analyze the light curves and estimate the exoplanetary orbital periods.

3.2.1 Obtaining the light curves

The equations shown in the previous subsection are based on the observables of a light curve (transit depth, transit duration and flat transit duration). We decided to test those equations using the light curves obtained by the Kepler Mission, as they are publicly available through easy access at the Mikulski Archive for Space Telescopes (MAST) ¹ and a large sample of exoplanets (more than 1000) has been discovered by this transit survey. Available data are classified into the different quarters and each system dataset is contained in the FITS format

¹<http://archive.stsci.edu/pub/kepler/lightcurves/tarfiles/>

archive. These archives contain several parameters describing each star and column listings of the individual photometric measurements, with their various parameters and quality flags. However, we are just interested in the time of measurement (column 1) and the flux measured (column 8), in order to reproduce the light curves and observe the possible planetary transits.

These measurements are stored by the Kepler Telescope in two different time cadences. One is the Long Cadence (LC), where the flux is measured every 30 minutes, and the other is the Short Cadence (SC), which measures the flux every minute. LC is mainly allocated to transiting planets search, as it provides a good photometric precision (50 ppm) in G2V stars with magnitude $k_p = 12$ ¹. On the other hand, SC is allocated to characterization of planetary transits, discovered by LC, and asteroseismology programs (Borucki et al. 2009). The two different cadences are a consequence of the limited telemetry availability and the need to define a trade-off between the number of downloaded CCD windows and their time frequency (i.e., many windows at LC and less windows at SC).

We need to mention that each system is identified by an ID integer number containing 8 digits, whereas in exoplanets data tables each system is identified by a name. We used the ‘Kepler names’ table in NASA Exoplanet Archive² in order to know which Kepler name corresponds to each Kepler ID.

3.2.2 Selecting a sample to work with

The sample of objects we select to carry out our study should be large enough to represent a statistically significant group and small enough so that its analysis requires a reasonable amount of time.

We decided to take the table data of the confirmed exoplanets discovered by Kepler Mission, which contained 1022 planets as of April 2015 and can be downloaded from the MAST website³. This table contains the data of our interest like the orbital period, transit depth, stellar parameters, among others.

Recall that the TESS Mission will cover most of the sky for only 28 days. Therefore is possible to detect a single planetary transit for systems with periods longer than 14 days in the resulting light curves. Also, we have shown that some of the approximations we use (Section 3.1) are worse when orbital periods are shorter. Thus we cut-off our sample at 14 days of orbital period. Since we do not want to keep a very large sample we also establish an upper boundary, which is selected to be 40 days. This way we can identify known planetary

¹<http://keplerscience.arc.nasa.gov/>

²<http://exoplanetarchive.ipac.caltech.edu/cgi-bin/TblView/nph-tblView?app=ExoTbls&config=keplernames>

³https://archive.stsci.edu/kepler/confirmed_planets/search.php

periods, looking at the corresponding light curves, with the measurements of flux contained in only one quarter (90 days). When setting this constraint the original catalog is reduced to 280 objects.

Because our sample is still large and transits with larger transit signal-to-noise ratio can be more accurately detected in the light curves, we decided to put a new constraint depending on the transit depth, keeping those planets producing transit depths higher than 1000 parts per million (ppm), according to the MAST table data. Applying this cut-off, our sample reduces to 63 objects, thus becoming a reasonable amount of systems to be analyzed.

The next step is to check the availability of the light curves for each of the systems we have kept. We have to consider that at long cadence format, flux is measured every 30 minutes and the ingress/egress transit period that we need to estimate is usually not longer, which means that we should use the short cadence format if we want to avoid the difficulties of joining several transits. However, for the reasons explained above, there are far less light curves available in short cadence than in long cadence, and the photometric noise is much larger in SC than in LC, as the photometric precision increases as the integration time also increases. As long as we want to analyze a sample in SC, we need to check for how many systems their light curves are available in this format. This can be done at NASA Exoplanet Archive ¹ by introducing the Kepler ID of the system which we want to search. We checked that, at least, a whole quarter is available for 51 of the 63 exoplanets that we had kept. Thus, we still had a statistically significant sample.

As it will be shown in next section, models obtained with JKTEBOP, working with the short cadence format, yield acceptable results for just one system. For this reason we decided to work also with the long cadence format, since a longer cadence results into a lower photometric noise. The use of long cadence data, however, implies the need of joining several transits, as the cadence is too long to resolve the ingress/egress regions of the light curves when considering just one transit event. The transits selected from the light curves obtained in long cadence format are joined by subtracting to their measurement time the amount of periods corresponding to the number of transits shifted from the first one. Because Q0 & Q1 are shorter than the following quarters and there are less stars available, we start taking transits from Q2, and they are taken in chronological order, unless we skip those transits that have a low transit signal-to-noise ratio or some measurement is missing.

We follow the same criteria as for the short cadence to select a sample to work with at long cadence, with the difference that this time we cut-off the sample at a depth of 2000 ppm, instead of 1000 ppm, since selecting and joining several transits requires an important

¹http://exoplanetarchive.ipac.caltech.edu/applications/ETSS/Kepler_index.html

amount of time for each system. Using these conditions we keep a sample of 22 planets and 20 host stars. However, there is one system whose light curve in LC is not used, as a light curve in SC of good quality exists.

The number of transits that we fold varies depending on the system. For all systems, we firstly join 6 transits. If its resulting light curve is not noisy in the sense that the transit can be clearly seen, we increase our selection up to 10 transits. If transit can be, still, seen with precision, we finally join a total of 15 transits. We decide to join these amount of transits, as they are translated into typical cadences of 5, 3 and 2 minutes, respectively. We consider that a cadence of 2 minutes is good enough if we want to analyze a transit in detail, in order to reach our goal, whereas a cadence of 5 minutes should be acceptable.

3.2.3 Modeling planetary transits

In order to determine the duration of the transits, ingress and egress times, we model transit light curves from the measurements of the flux we downloaded for each system. The modeling of such light curves is performed using a program known as JKTEBOP (Southworth 2012). JKTEBOP is a code based on FORTRAN language, written by John Southworth¹. This program was developed to model the light curves produced by eclipsing binaries, composed of two stars (referred as star A & star B in JKTEBOP) orbiting each other, but is also applicable for planets orbiting a central star. In this case of being the small body a planet, the usual convection is that star A corresponds to the central star and star B corresponds to the planet.

JKTEBOP reads several input parameters that the user introduces. The parameters we consider are the sum of the stellar and planetary radii, normalized in terms of the orbital semi-major axis, the radii ratio between both bodies, the orbital inclination, the orbital period, the LD, the time of minimum light (TML) and the phase shift, related to the time of minimum light. The input parameters can be fixed to an initial value, or can be left free to be adjusted by JKTEBOP and then returned as output parameters with a new converged value. In the test runs we model the light curves fixing the orbital period, as well as the time of minimum light and the stellar limb darkening. In contrast, we left free to be adjusted the sum and ratio of radii, the orbital inclination and the phase shift.

The program, also, reads an input file containing the measurements of flux, which are formatted in terms of normalized magnitudes. Then, it finds by several iterations an output model that best fits the data, taking into account the input parameters, introduced by the user, and the measurements of the flux. JKTEBOP outputs 3 different files. The first one contains the input magnitudes, the magnitudes given by the output model, for each measurement,

¹<http://www.astro.keele.ac.uk/jkt/codes/jktebop.html>

and the residual values (observed minus calculated). The second file includes the magnitudes of the output model given as a function of the phase shift. Finally, a third file contains the input and output (adjusted) parameters.

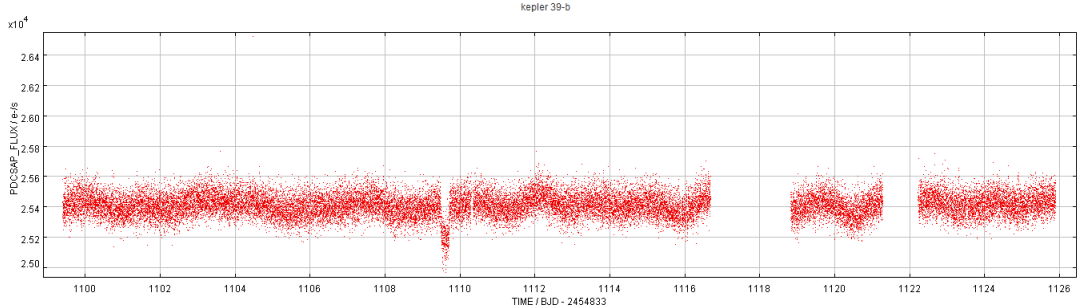


Figure 3.2: Light curve downloaded from MAST.

Before running JKTEBOP, we need to convert the measured flux units (erg/s) to normalized magnitudes. This is carried out by, firstly, selecting a window of the light curve around the transit event (Figures 3.2 & 3.3) and then removing the transit (Figure 3.4). Once the transit is removed, we normalize the flux to 1. In some cases the flux is not constant and clearly trend appears. This is because many stars have surface spots that cause brightness variations as the star rotates. Thus, the normalization is done by a linear regression of the remaining points outside the transit and dividing all measurements by its corresponding value in function of the time (Figures 3.4 & 3.5). After that, the normalized flux is converted into magnitudes by using expression (3.10). This leads to an average value of 0 magnitudes outside the transit and positive magnitude values inside.

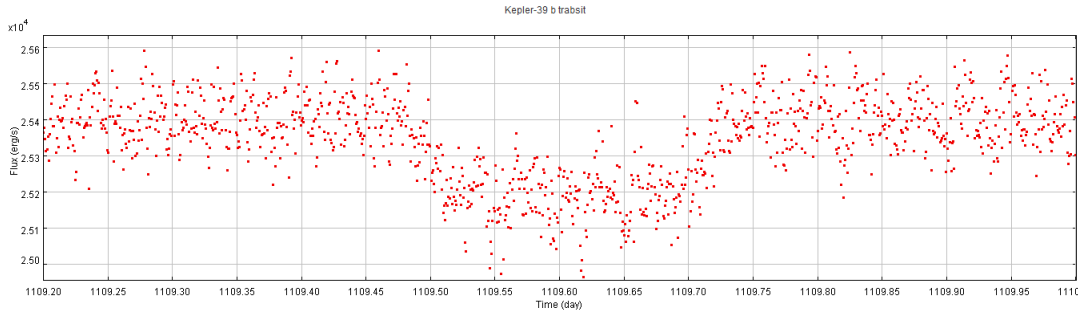


Figure 3.3: Transit region amplified from the light curve.

$$m - m_0 = -2.5 \log \frac{F}{F_0} \tag{3.10}$$

Most of orbital input parameters, introduced into JKTEBOP, are taken from the data table downloaded from MAST, while the LD of the central star (star A in JKTEBOP) is estimated

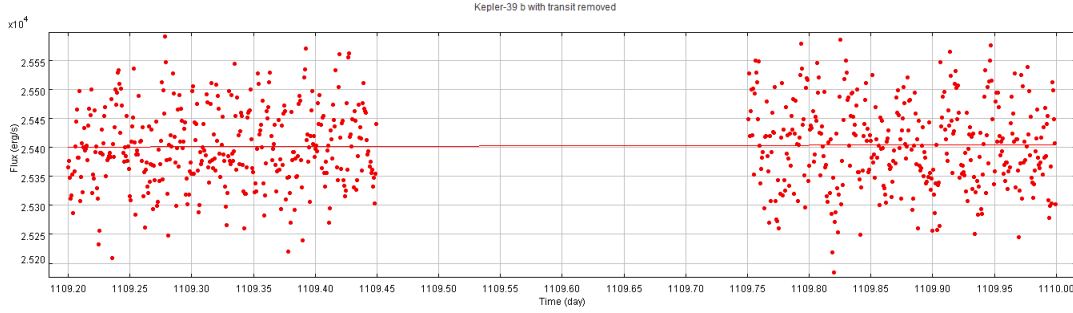


Figure 3.4: Linear regression of the measurements in the neighborhood of the transit region with transit removed.

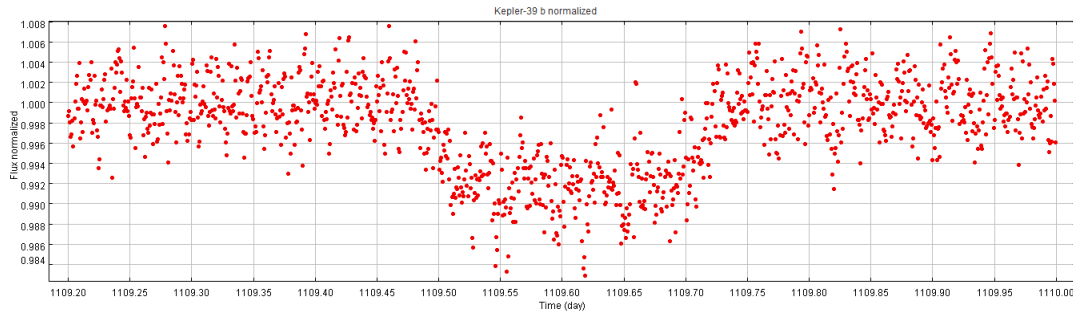


Figure 3.5: Transit represented in terms of the normalized flux.

as a function of the effective temperature by looking at the table by Sing (2010), where LD coefficients for the Kepler band can be found. JKTEBOP allows to use the linear, quadratic, cubic, square or logarithmic LD laws, but only the linear coefficient and a non-linear LDC can be introduced at the same time. We decided to use the quadratic LD law, since it is the most commonly employed one, due to its simple, intuitive form and it is applicable to a wide sample of stellar effective temperatures (Kipping 2013). A quadratic LD law includes a linear term and a quadratic term. We fix the LD coefficients of the host star to the tabulated values.

3.2.4 Taking our output results

Once JKTEBOP is run, we can show our output models and estimate the orbital periods using a single transit.

We plot the output model together with the measurements of flux and the characteristic times of the transit. These times are t_1 , which corresponds to the beginning of the transit, t_2 , the transition between ingress and flat transit, t_3 , the transition between flat transit and egress, and t_4 , the end of the transit (see Figure 3.1). All plots are performed using the TOPCAT

software ¹.

The flux measurements were taken from the input file downloaded from MAST. The model curve was taken from the output file provided by JKTEBOP. Finally, the transit times are estimated by finding the points of the model light curve with sudden slope changes. Since the measurements in the Kepler database are shown as a function of time (day of measurement) and JKTEBOP outputs the magnitudes associated to the model as a function of the orbital phase, we convert this phase into time by multiplying the phase by the input orbital period and summing to that value the time of minimum light. In some cases it may be difficult to estimate t_2 and t_3 (beginning and end of the flat transit) just by looking the slope of the fit curve, so what we do is to run JKTEBOP again by adopting a hypothetical LD = 0 and fixing all output parameters given by the model with LD. This way we can easily determine all characteristic transit times (because the central part of the transit is completely flat), without changing the rest of the physics of the system. All these files containing data to be plotted are converted to ASCII format to be read by TOPCAT.

Although the data tables downloaded from MAST include the transit depths, we decided to measure our own depths using our models. We carried out the depth determination by taking the mean magnitude of the points located in the flat transit region (between t_2 and t_3) and then their values, in difference of magnitude with respect to 0, are reconverted into fraction (ppm) again by inverting Equation (3.10). This conversion is carried out in order to calculate the orbital planetary period using Equation (3.9).

$$F = 10^{\frac{-m}{2.5}} \quad (3.11)$$

As we shown in Equation (3.9), the estimate of the period strongly depends on some key stellar parameters, in particular, on the stellar radius, as it depends as its cub. We take the stellar parameters from 3 different sources: The Extrasolar Planet Encyclopedia ², NASA Exoplanet Archive ³ and Open Exoplanet Catalog ⁴. We choose the stellar masses and radii from the source we consider their measurements are the most accurate, typically the parameters with the smallest uncertainty. In next section a small discussion is performed about the stellar parameters chosen for each system.

3.2.5 Errors taken into account and its propagation error formulas

We consider two error sources for the characteristic transit times. One is associated to the precision of the measurements and is defined as the typical distance in time between two

¹<http://www.star.bris.ac.uk/~mbt/topcat/>

²<http://exoplanet.eu/catalog/>

³<http://exoplanetarchive.ipac.caltech.edu/cgi-bin/TblView/nph-tblView?app=ExoTbls&config=planets>

⁴<http://www.openexoplanetcatalogue.com/systems/>

measurements of the flux. This is calculated as the typical interval between photometric measurements of the long/short cadence divided by the number of transits joined. The other error is caused by the random noise (RMS) that is present in the flux measurements and that has various sources (target brightness, crowding, telescope pointing jitter, etc). This error is considered to be proportional to the RMS-to-depth ratio and it is normalized by multiplying this ratio by the ingress/egress duration. We provide a image of a light curve analyzed, in order to ease the understanding of this explanation (Figure 3.6). The expressions for the final error of the times are the Equations (3.12) & (3.13), where the left terms correspond to the cadence error and the right term is the error associated to the RMS. Note that the quadratic sum stems from the assumed uncorrelated nature of the two error sources.

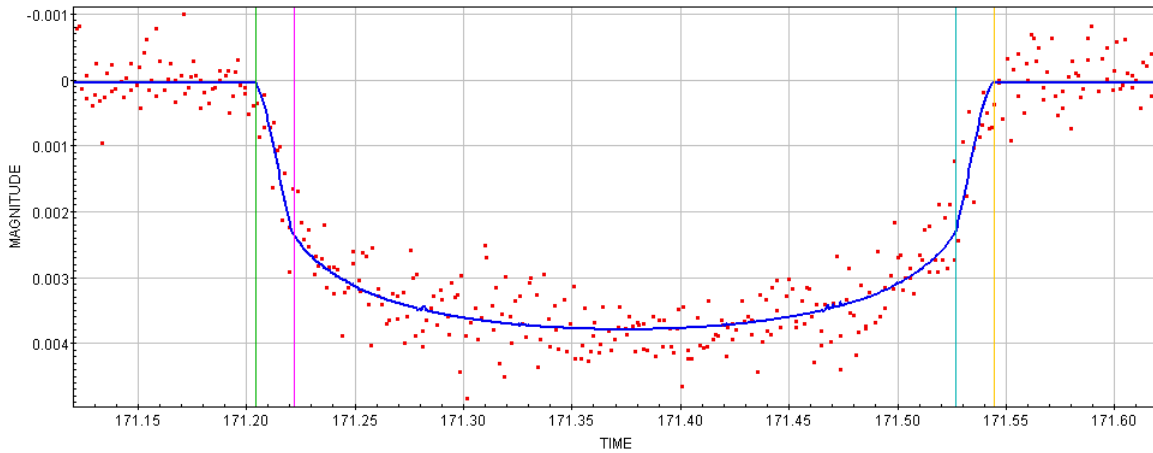


Figure 3.6: Model fit for the Kepler-238 e light curve. Measurements are in long cadence, with 15 transits joined.

$$\sigma_{t_{1,2}} = \sqrt{\left(\frac{\text{Cadence length}}{N \text{ transits}}\right)^2 + \left(\frac{\text{RMS}}{\Delta F}(t_2 - t_1)\right)^2} \quad (3.12)$$

$$\sigma_{t_{3,4}} = \sqrt{\left(\frac{\text{Cadence length}}{N \text{ transits}}\right)^2 + \left(\frac{\text{RMS}}{\Delta F}(t_4 - t_3)\right)^2} \quad (3.13)$$

The error in the depth is estimated by considering the error of the difference between the normalized flux and the flux inside flat transit:

$$\sigma_{\Delta F} = \sqrt{\text{RMS}^2 + \text{RMS}_{t_F}^2} \quad (3.14)$$

And these uncertainties are calculated in fraction of the flux with the derivation of Equation (3.11) for RMS and RMS_{t_F} :

$$\sigma_F = \frac{\ln 10}{2.5} 10^{\frac{-m}{2.5}} \sigma_m = \frac{\ln 10}{2.5} F \sigma_m \quad (3.15)$$

Duration of transits and flat transits are also estimated by calculating the quadratic sum of the time uncertainties:

$$\sigma_{t_{T,F}} = \sqrt{\sigma_{t_{4,3}}^2 + \sigma_{t_{1,2}}^2} \quad (3.16)$$

With the aim to carry out the calculation of the final error of the period, we compute the error of the factor $(t_T^2 - t_F^2)^{3/2}$. This error is computed asymmetrically because the relative error can be very large, since we are doing a quadratic subtraction and t_T & t_F are often quite similar when the transit is very central. Thus, we cannot use the typical error propagation formula. We define t_*^+ & t_*^- as:

$$t_*^\pm = t_* \pm \frac{\sigma_{t_*}}{\sqrt{2}} \quad (3.17)$$

Then we consider σ_+ , associated to this factor, to be the difference with respect to the main value, when we apply t_T^+ & t_F^- to the factor formula, whereas σ_- is considered applying t_T^- & t_F^+ .

Similarly, the dependence of the calculated orbital period with the stellar radius is very relevant and, often, the relative error is high. Thus, we also compute error contribution asymmetrically. Before doing that, we calculate the error of the factor $\frac{G\pi}{32} \frac{(t_T^2 - t_F^2)^{3/2}}{\Delta F^{3/4}} M_*$, which we represent as P_{noR} . Since the depth and mass dependences are small (and linear), we compute this error by the typical propagation formula, which results into:

$$\sigma_{P_{noR}} = P \left[\sqrt{\left(\frac{\sigma_{(t_T^2 - t_F^2)^{3/2}}}{(t_T^2 - t_F^2)^{3/2}} \right)^2 + \left(\frac{\frac{3}{4} \sigma_{\Delta F}}{\Delta F} \right)^2 + \left(\frac{\sigma_{M_*}}{M_*} \right)^2} \right] \quad (3.18)$$

$\sigma_{P_{noR}}$ is asymmetric, since the error of the factor $(t_T^2 - t_F^2)^{3/2}$ is also asymmetric. We define the upper and lower error boundaries of P_{noR} and R_* analogously to the way we defined the error boundaries for t_T and t_F (Equation 3.17). Then we consider that we obtain σ_P^\pm as shown in Equations (3.19) & (3.20):

$$P^+ = P + \sigma_P^+ = \frac{P_{noR}^+}{R_*^{3-}} \quad (3.19)$$

$$P^- = P - \sigma_P^- = \frac{P_{noR}^-}{R_*^{3+}} \quad (3.20)$$

4 Results and discussion

We provide a list of the systems (Table 4.1), with some of the most relevant parameters, whose light curves have been analyzed in detail. The values of these parameters correspond to the data available in MAST database.

Kepler	Radius (R_{\oplus})	Transit Duration (h)	Period (days)	Transit Depth (ppm)
18 d	5.96	3.492	14.86	3343.9
26 c	2.82	2.097	17.25	2247
27 b	4.94	3.575	15.33	3411.6
27 c	7.24	5.228	31.33	5679.3
31 b	5.28	5.149	20.86	2031.4
39 b	14.77	5.936	21.09	9318.5
89 d	9.77	6.686	22.34	5675.2
117 b	6.04	7.27	18.80	2483.8
118 c	7.19	3.126	20.17	5676.4
149 b	3.77	5.09	29.20	2108.3
222 d	3.75	4.525	28.08	2016.6
229 c	5.27	3.546	16.07	5317.1
230 b	3.79	6.364	32.63	2071.8
238 e	5.71	8.216	23.65	3573.4
247 d	5	3.538	20.48	2903.5
248 c	4.29	4.06	16.24	2734.9
257 d	5.67	2.97	24.66	2624.9
281 c	5.39	7.008	36.34	2932.6

Table 4.1: List of the transiting exoplanets, with their relevant parameters, whose light curves will be fitted to be analyzed. All these values belong to the Kepler catalog.

We will start analyzing the sample of systems observed at short cadence, and then we will carry on discussing those transits analyzed at long cadence. In all following plots, red points represent the measurements of fluxes, blue lines correspond to the fluxes given by the models, and t_1 , t_2 , t_3 & t_4 are marked with the green, pink, turquoise and yellow vertical lines, respectively. Finally, we will provide a table showing a summary of the obtained parameters to be compared to the real ones.

4.1 Systems analyzed with Short Cadence format

The Short Cadence format presents the great advantage that measurements are taken every minute, which means that by analyzing a unique transit we should have sufficient precision

to estimate the characteristic transit times. However, as the duration of the integration is very short, the measurement noise may be higher and therefore hamper a good fit of the light curve. Because of this, only very bright exoplanet hosts will have short cadence light curves of sufficient precision to apply our procedure. Actually, we analyzed just a handful of 51 systems selected and we have obtained a good fit only for system Kepler-89 d, which is discussed next.

4.1.1 Kepler-89 d

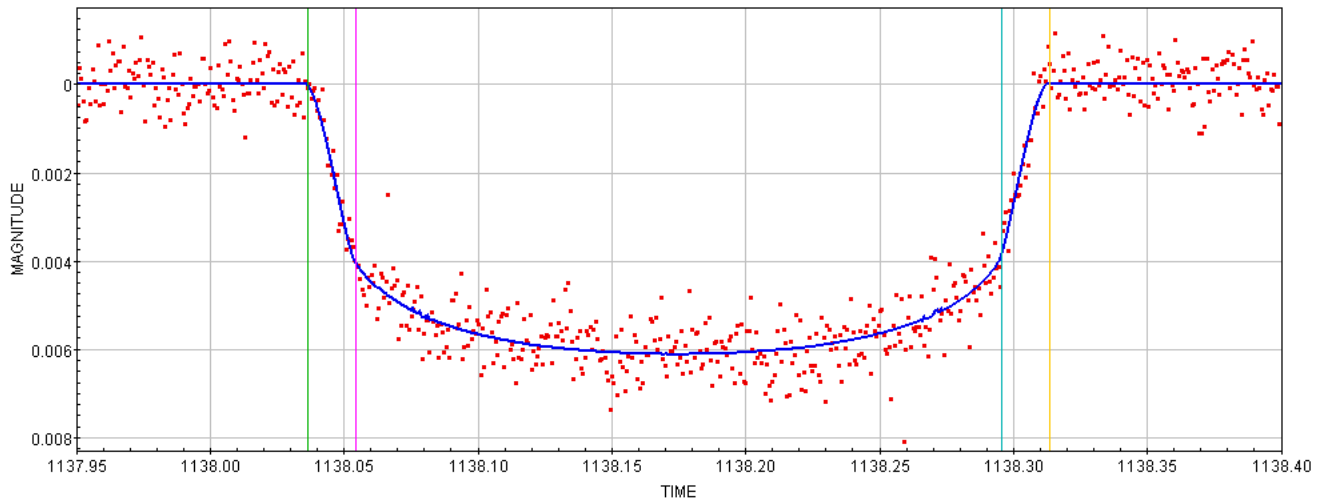


Figure 4.1: Model fit for Kepler-89 d light curve. Measurements are in short cadence and a single transit is considered.

Kepler-89 d is the only system whose light curve is reasonably well fitted by JKTEBOP if we use the light curve obtained at short cadence, being in good agreement with the measurements during the entire transit, as well as with the ingress/egress and flat transit light curve shape (Figure 4.1). This is possible because the transit depth is clearly significant when compared with the RMS.

4.1.2 Other cases

Here we show a few of the other cases, for which the analysis of the transits yields unreliable results. This is mostly explained by the large random noise measured at short cadence. Some examples are shown in Figures 4.2, 4.3, 4.4 & 4.5.

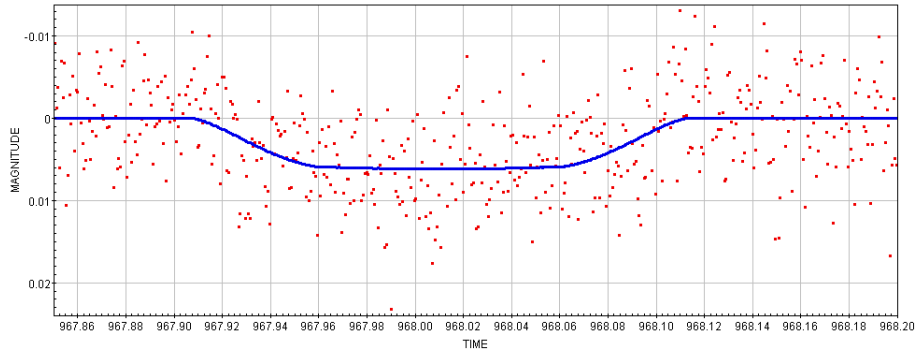


Figure 4.2: Model fit for Kepler-27 c light curve. Measurements are in short cadence and a single transit is considered.

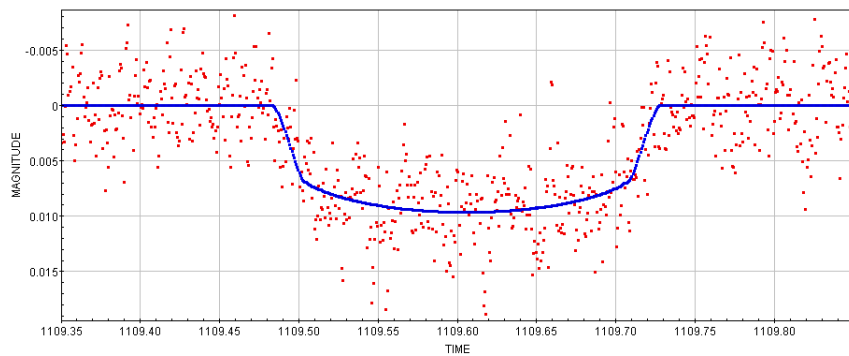


Figure 4.3: Model fit for Kepler-39 b light curve. Measurements are in short cadence and a single transit is considered.

The orbital period depends on the square of the quadratic difference between the transit duration and the flat transit duration, raised to the third power (Equation 3.9). This means that systems associated to light curves that cannot be modeled with high precision (Figures 4.2, 4.3 & 4.4) cannot be properly analyzed by this method, so their derived periods may become very unreliable. This may happen even when the uncertainties of the transit times given by the models seem to be relatively small, as it is the case shown in Figure 4.3, where the light curve can be intuited with higher precision than for the rest of systems shown. For this reason, we need to determine the transit times with very good precision and accuracy, so unless we obtain a good model fit, we will not be able to obtain a reliable orbital period.

Most of the rest of the sample in short cadence contains light curves that are so noisy that the transits are nearly indistinguishable, which causes JKTEBOP to yield numerically unrealistic results and fits. This is the case of Kepler-248 c, for example (Figure 4.5).

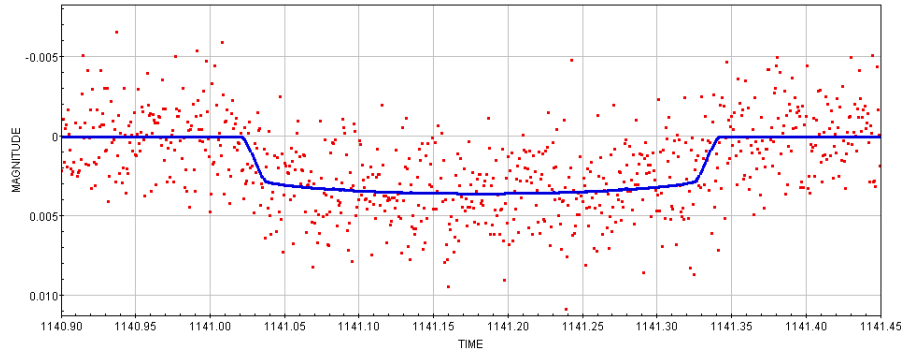


Figure 4.4: Model fit for Kepler-238 e light curve. Measurements are in short cadence and a single transit is considered.

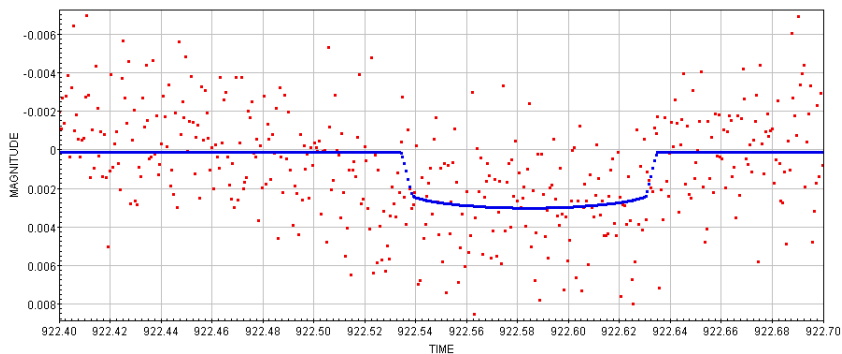


Figure 4.5: Model fit for Kepler-248 c light curve. Measurements are in short cadence and a unique transit is considered.

4.2 Systems analyzed with Long Cadence format

Given the fact that only one short cadence light curve could be used, we decided to increase the number of objects under study, by including those with long cadence measurements. In these cases, the RMS should be smaller as the duration of the integration is longer.

Working with long cadence data comprises additional steps, since it requires joining several transit events in order to have the ingress/egress transit curve sufficiently well defined. In contrast, the main advantage is that the flux error is significantly smaller, which allows to determine the transit parameters with better precision.

As explained in the previous chapter, we have selected a sample of 22 systems to be analyzed with long cadence. However, there is one (Kepler-89 d) that will not be analyzed, since its transit has been properly modeled using its light curve in short cadence. Some of the remaining 21 systems are also discarded as it is explained next.

Two of the removed systems are Kepler-46 b and Kepler-9 b. These systems have transit timing variations (TTV), which means that their orbital periods are changing with time due to gravitational perturbations caused by other possible companions. In these cases, the effect of folding several transits is what it can be seen in Figures 4.6 & 4.7. Transits do not start and finish at the same orbital phase. Obviously, these light curves are not reliable because the most probable is to obtain a light curve modeled with poor precision at the time of fitting the transit. Also, the same perturbations that cause deviations in the central transit time could be causing variations in the transit duration, which would render the parameters determined from the light curve fits unreliable.

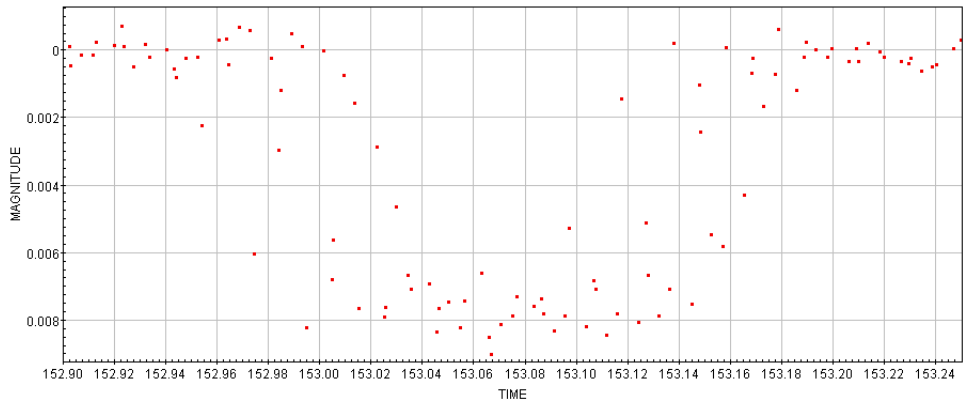


Figure 4.6: Folded Kepler-46 b light curve. Measurements are in long cadence, with 6 transits joined.

Another system removed from our analysis is Kepler-9 c, for being an extreme case of TTV system. We consider that is not worth including its corresponding plot, as the dispersion of their transits is too large to distinguish any transit. Finally, we decide to discard Kepler-32 c, since the RMS is nearly of the same order of the transit depth, so we assume that the output model would be likely of low precision.

From these considerations, we have discarded a total of 4 systems, keeping a final sample of 17 light curves obtained in long cadence.

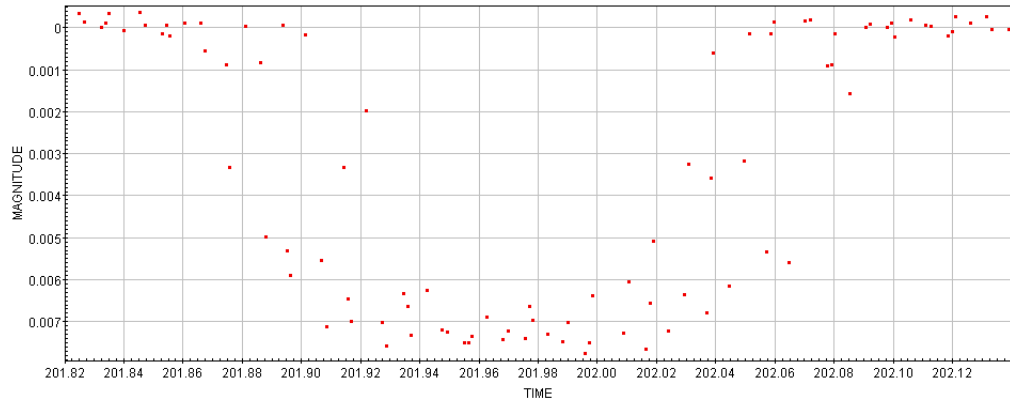


Figure 4.7: Folded Kepler-9 b light curve. Measurements are in long cadence, with 6 transits joined.

4.2.1 Kepler-18 d

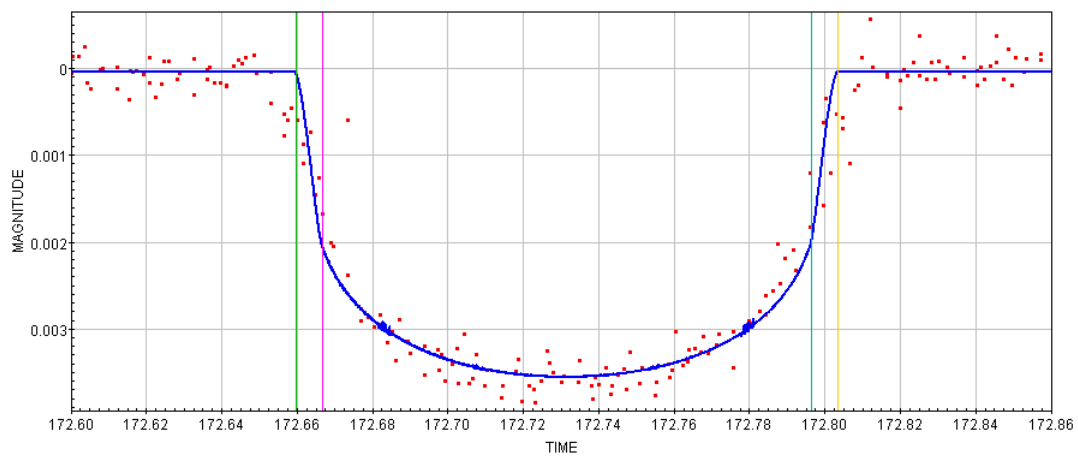


Figure 4.8: Model fit for the Kepler-18 d light curve. Measurements are in long cadence, with 15 transits joined.

The fit for the system is not good, and the ingress/egress lengths appear shorter in the model (Figure 4.14). Despite having the measurements uniformly distributed and being the RMS quite small, the slopes are sufficiently away from the model to consider this fit as poor.

4.2.2 Kepler-26 c

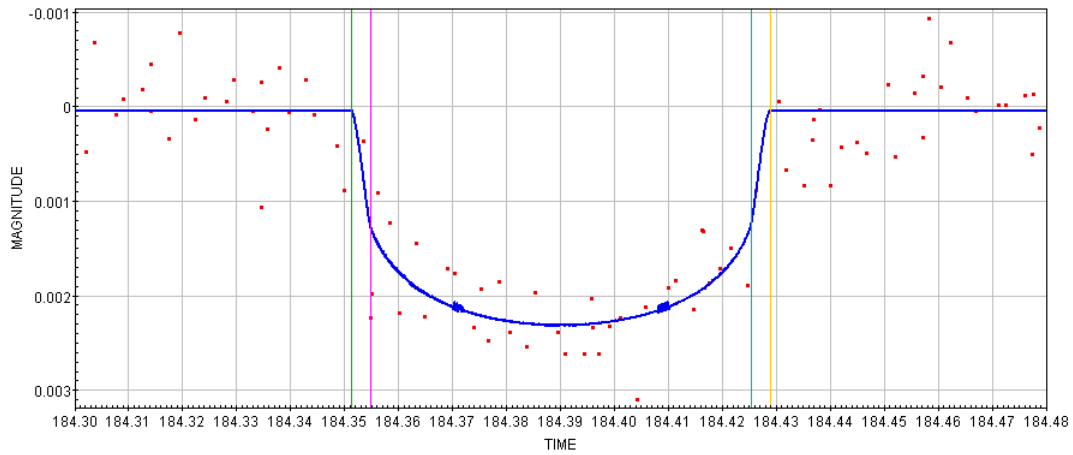


Figure 4.9: Model fit for the Kepler-26 c light curve. Measurements are in long cadence, with 10 transits joined.

This system seems to have some level of TTVs, since two different transit shapes become apparent when looking at the light curve (Figure 4.20). This creates uncertainty on the model and its ingress/egress slopes are shorter than what the measurements seem to suggest. For these reasons, the fit of this model cannot be considered good enough to be analyzed in detail.

4.2.3 Kepler-27 b

The measurements present, in this case, a significantly higher RMS-to-depth ratio (Figure 4.13) than the other systems previously studied. However, the fit does not seem affected and the model provides a good description of the measurements. Furthermore, transit and flat transit durations of the model agree well with the measurements, as well as the ingress/egress slopes.

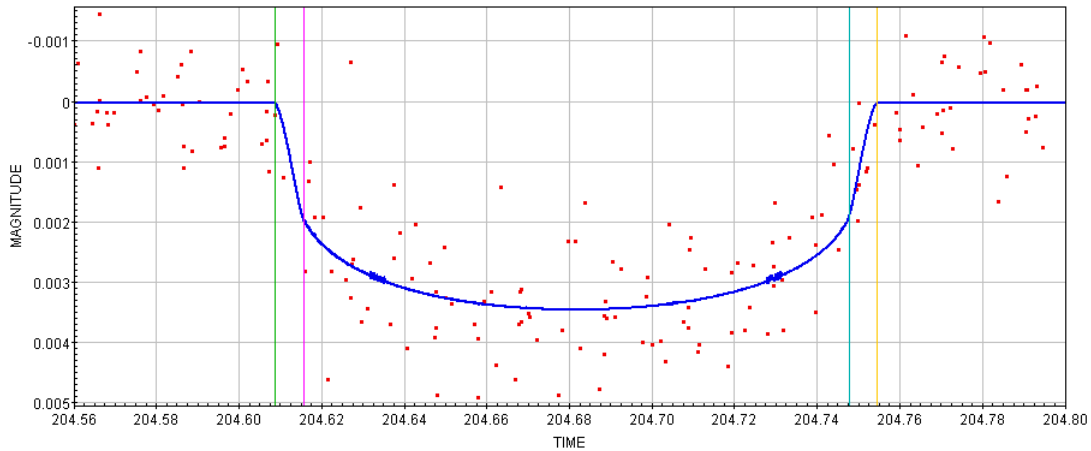


Figure 4.10: Model fit for the Kepler-27 b light curve. Measurements are in long cadence, with 15 transits joined.

4.2.4 Kepler-27 c

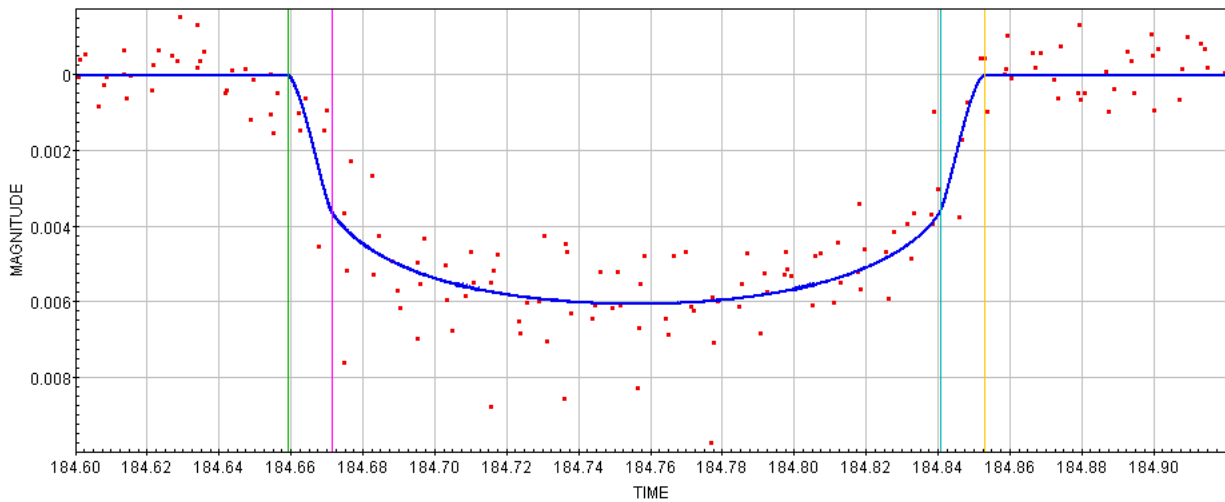


Figure 4.11: Model fit for the Kepler-27 c light curve. Measurements are in long cadence, with 10 transits joined.

The measurements of flux for the system Kepler-27 c have a significantly large RMS-to-depth ratio, and this is the reason because we have decided to stop adding transits after joining 10 transits. We consider that this high RMS most probably explains the fact that the ingress slope does not seem to be accurately reproduced if we observe the flux measurements (Figure 4.9). However, this does not seem to be a problem since the egress slope of the model is in very good agreement with the measurements and both sides are supposed to

be symmetric. This way we discard this system to be a TTV system and we assume that the light curve fit is good.

4.2.5 Kepler-31 b

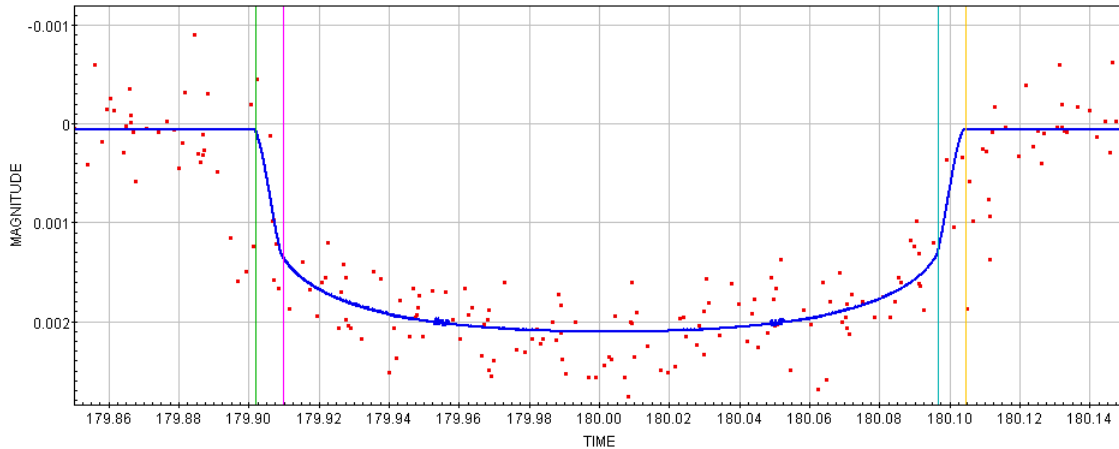


Figure 4.12: Model fit for the Kepler-31 b light curve. Measurements are in long cadence, with 15 transits joined.

The RMS-to-depth ratio is also large for this transit light curve. In this case, the random noise makes the agreement of the ingress/egress slopes unclear, as well as the duration of the transit, whose measurements suggest that it should be longer (Figure 4.23). This makes us consider this model fit quite poor.

4.2.6 Kepler-39 b

Kepler-39 b is the confirmed exoplanet having the deepest transit of our sample. The model light curve seems to fit well observed light curve, although the measurements seem to cluster instead of being uniformly dispersed after folding the transits (Figure 4.8). This is likely due to the commensurability of the orbital period with the 30-min measurement cadence. The only trouble is that the characteristic transit times are found far from any point of measurement, providing larger uncertainties of the times than the considered uncertainties, basing on our criteria (Section 3.7). However, this does not seem to be an important problem, and also, looking at its light curve, the ingress/egress slopes seem to be very well defined.

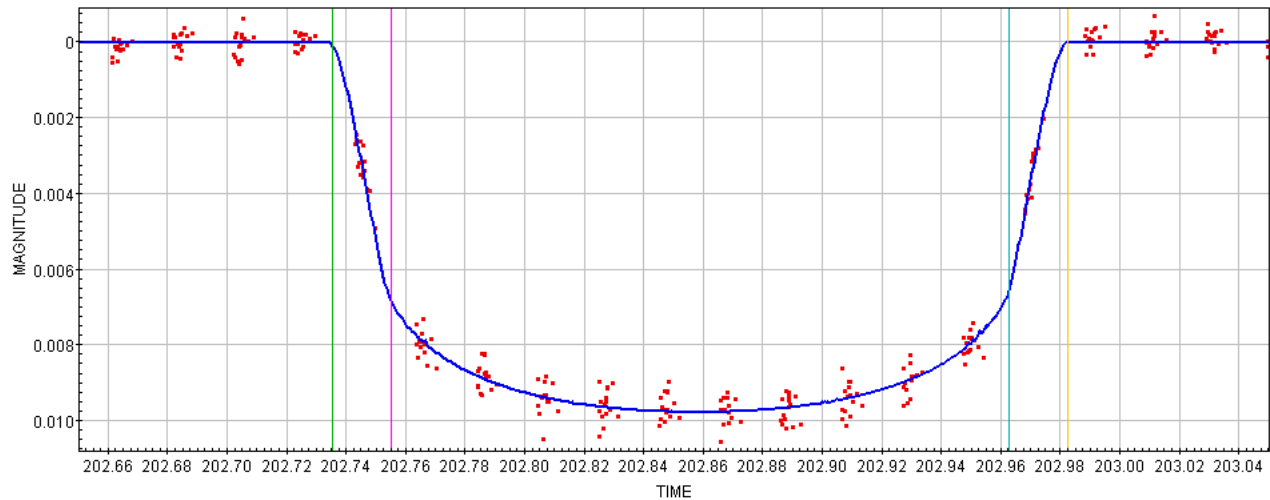


Figure 4.13: Model fit for the Kepler-39 b light curve. Measurements are in long cadence, with 15 transits joined.

4.2.7 Kepler-117 b

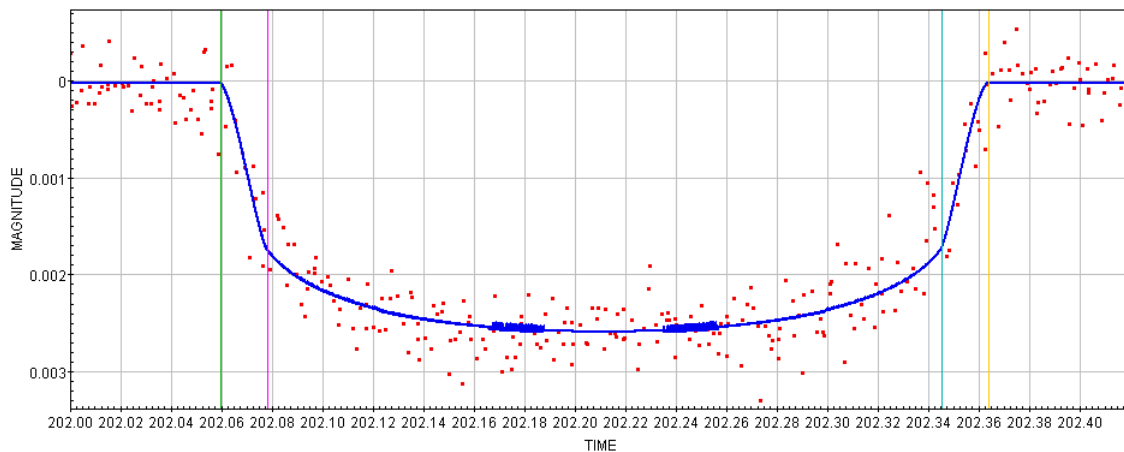


Figure 4.14: Model fit for the Kepler-117 b light curve. Measurements are in long cadence, with 15 transits joined.

This model behaves in a similar way to the systems Kepler-27 c & Kepler-248 c, in which one of the ingress/egress slopes does not exactly correspond to the measurements, whereas the other one does. In this case the egress slope agrees with the measured curve with precision, whereas the random noise generates certain uncertainties on the ingress slope (Figure 4.19). However, as in the previous cases, this fact does not alter significantly the reliability of the model.

4.2.8 Kepler-118 c

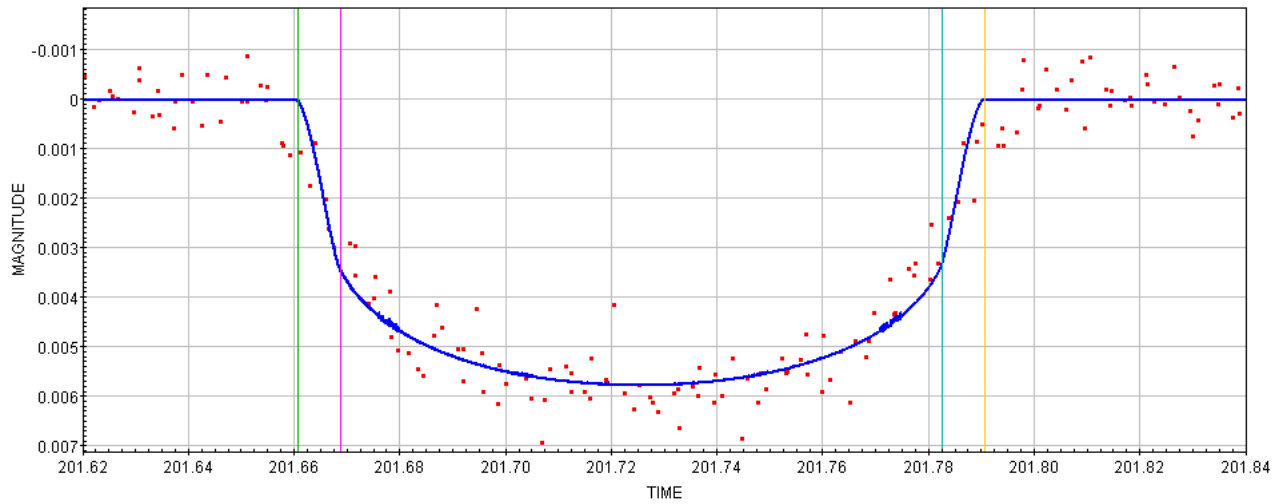


Figure 4.15: Model fit for the Kepler-118 c light curve. Measurements are in long cadence, with 15 transits joined.

This is a clear example where the fitting algorithm has not worked properly. Although the measurements are distributed uniformly and the RMS-to-noise ratio is reasonably good (Figure 4.10), the ingress/egress model slopes are different to the observed light curve and their durations seem to have been considerably shortened by the model. For this reason this model cannot be considered as a reliable fit, so its derived period is expected to be much shorter than the real one.

4.2.9 Kepler-149 b

For this system we have selected only 6 transits because most of the measurements fall very close to the others in the phase space, forming clusters with long gaps between them. So we decided to take just the most dispersed transits (Figure 4.21). The light curve fit shows quite good agreement with the measurements, thus providing a good model, with the transit duration and the ingress/egress slopes well defined.

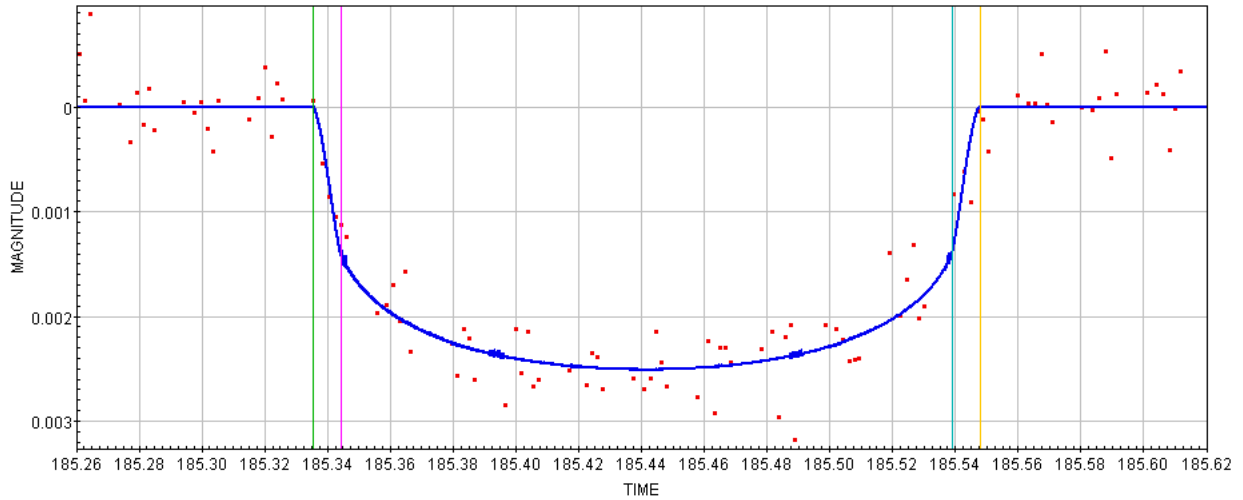


Figure 4.16: Model fit for the Kepler-149 b light curve. Measurements are in long cadence, with 6 transits joined.

4.2.10 Kepler-222 d

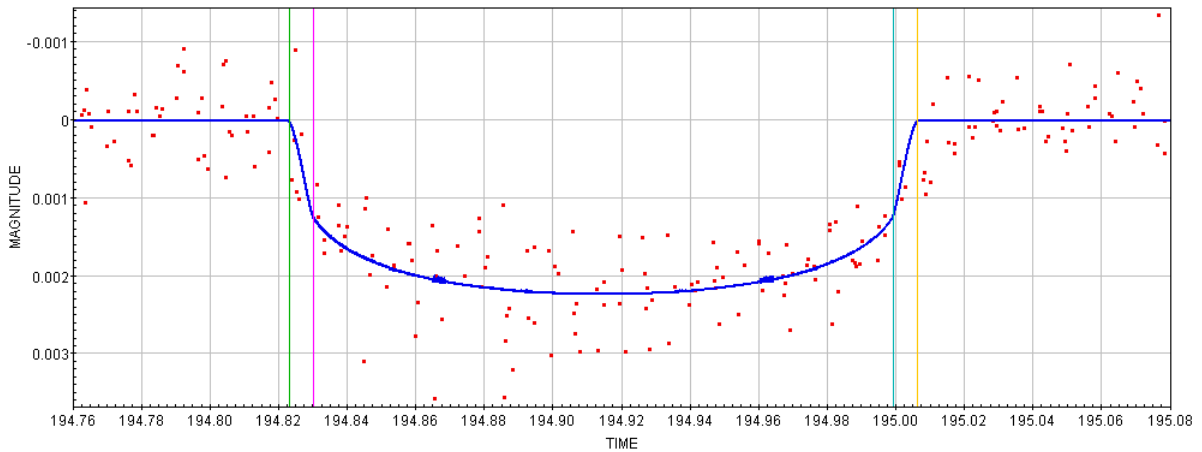


Figure 4.17: Model fit for the Kepler-222 d light curve. Measurements are in long cadence, with 15 transits joined.

For this last case, the RMS-to-depth ratio is, also, quite large, as in the two previous cases. However, the random noise does not seem to produce a model presenting significant deviations with respect to the measurements, showing a quite good agreement with the transit duration (Figure 4.24). The only drawback is that the ingress/egress slopes seem to present discrete deviations with respect to the light curve, looking like slightly shorter than expected. For these reasons we consider that the reliability of this fit is moderate.

4.2.11 Kepler-229 c

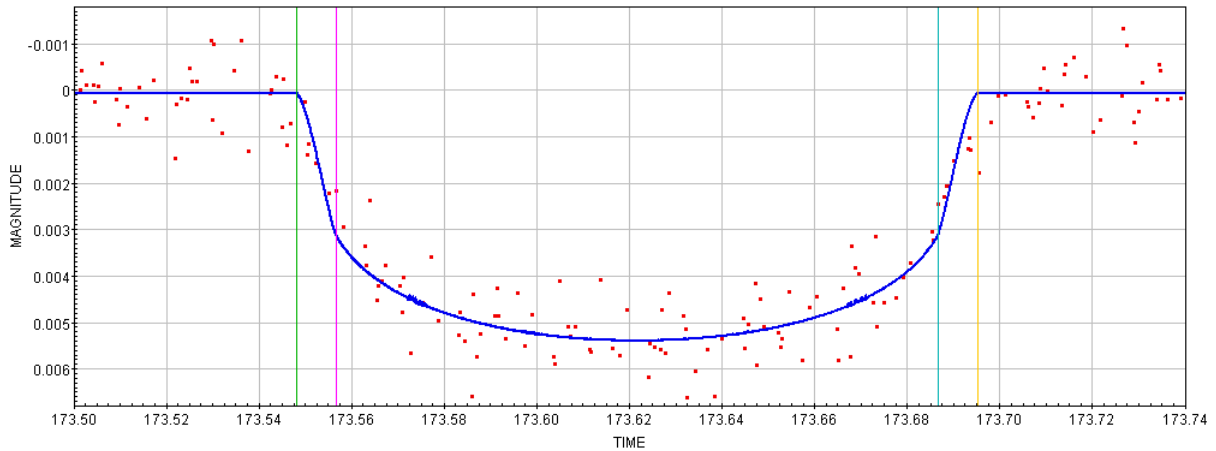


Figure 4.18: Model fit for the Kepler-229 c light curve. Measurements are in long cadence, with 15 transits joined.

The model seems, a priori, to fit quite well the light curve of this system. However, small deviations can be observed with respect to the measurements (Figure 4.11). These deviations may be attributed to random noise, but also to a failure of the algorithm, since the modeled light curve seems to indicate a slightly shorter transit when compare with the measurements. Due to these small uncertainties and lack of precision, this output model is considered moderately reliable at the time of interpreting the results.

4.2.12 Kepler-230 b

This light curve (Figure 4.22) has a large RMS-to-depth ratio but this does not seem to affect significantly the fit of our model, showing its ingress/egress slopes a good agreement with what can be deduced from the measurements. There are no clear evidences of TTVs, either. What it is not absolutely clear is the correspondence of t_1 , t_3 & t_4 to the measurements, suggesting that both transit and flat transit duration should be slightly larger than what the model indicates. Taking into account these assumptions, we consider that the fit for this system is moderately reliable.

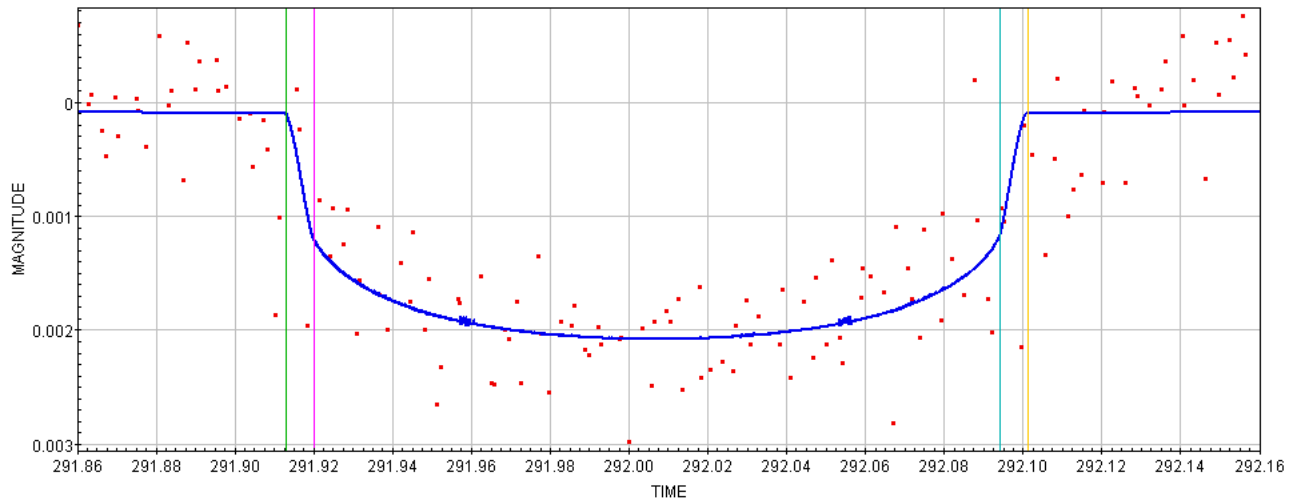


Figure 4.19: Model fit for the Kepler-230 b light curve. Measurements are in long cadence, having joined 10 transits.

4.2.13 Kepler-238 e

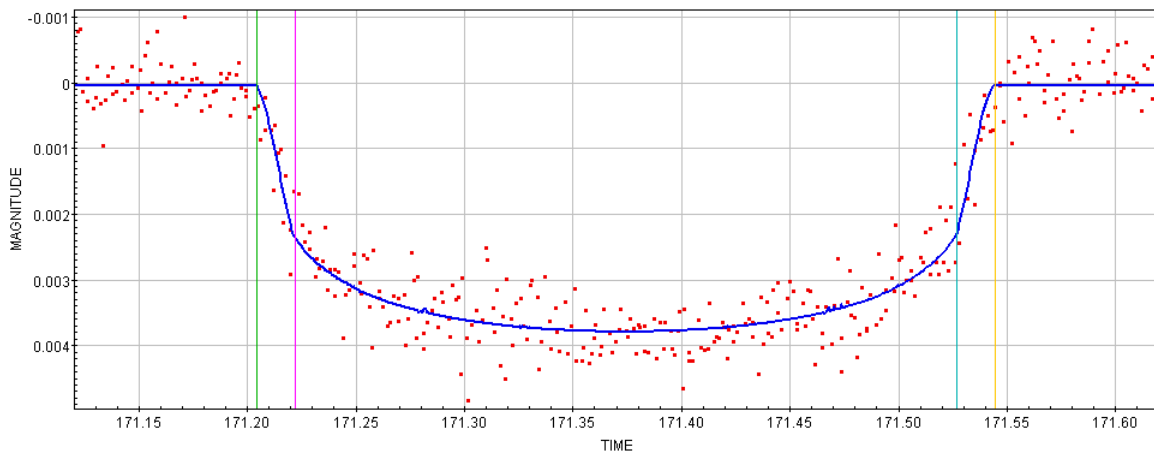


Figure 4.20: Model fit for the Kepler-238 e light curve. Measurements are in long cadence, with 15 transits joined.

The fitted model is in good agreement with the measured light curve for this system, without showing significant deviations with respect to the observed light curve (Figure 4.12). The transit duration and the ingress/egress slopes are very well defined, too.

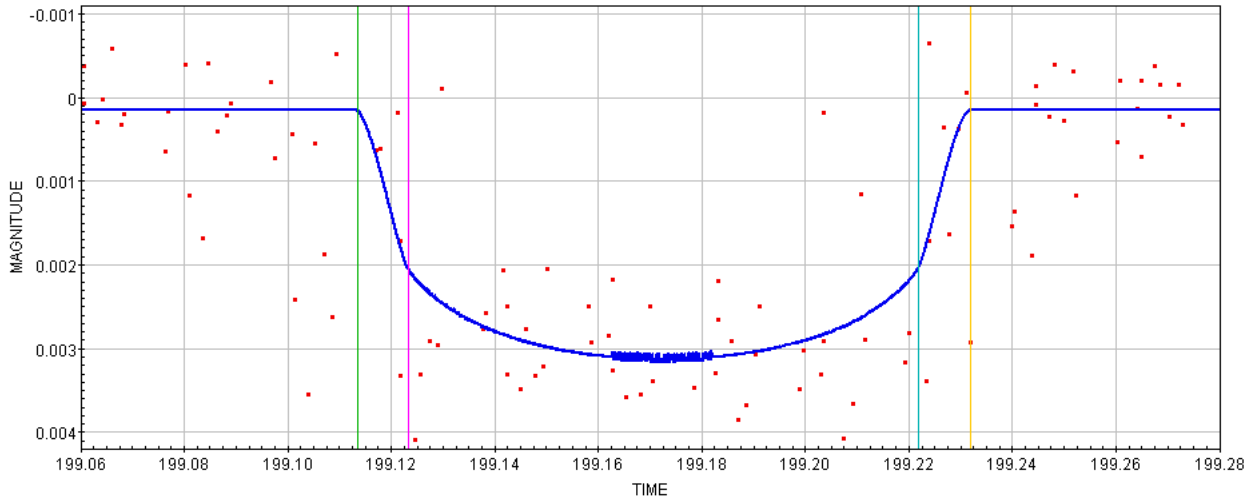


Figure 4.21: Model fit for the Kepler-247 d light curve. Measurements are in long cadence, with 10 transits joined.

4.2.14 Kepler-247 d

The light curve of this system is quite noisy and this may partly be due to the folding of the transits. This light curve presents the typical characteristics of a system with TTVs (Figure 4.16), since several transits starting at different orbital phases are observed from the light curve. For these reasons, the model cannot be determined with proper precision and the results obtained for this exoplanet will not be highly reliable.

4.2.15 Kepler-248 c

The transit seems well fitted in this case, with well-defined transit duration and ingress/egress slopes (Figure 4.17). The random noise does not significantly alter the model with respect to the measurements and we consider that the small uncertainties that appear on the egress slope are caused by the RMS, since the ingress slope agrees very well and both sides are supposed to be symmetric.

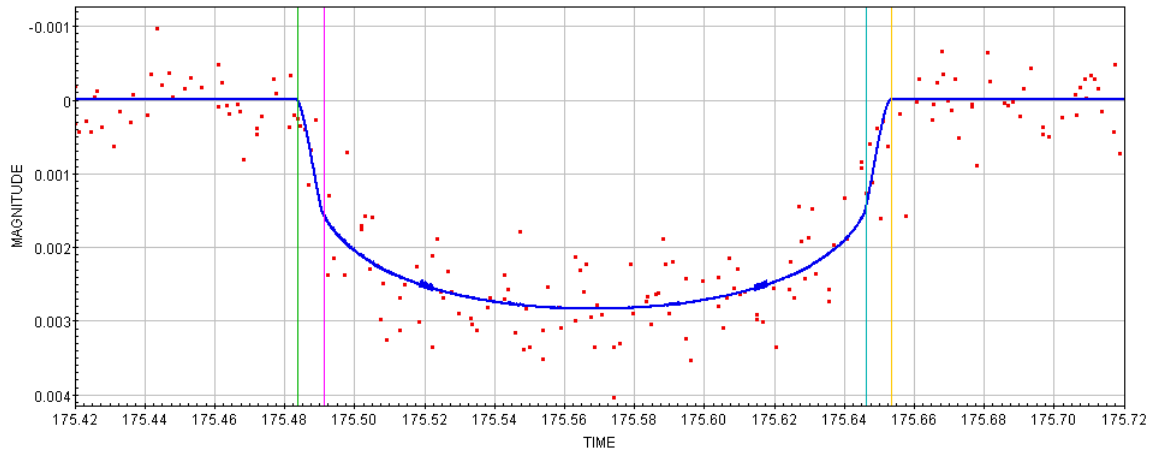


Figure 4.22: Model fit for the Kepler-248 c light curve. Measurements are in long cadence, with 15 transits joined.

4.2.16 Kepler-257 d

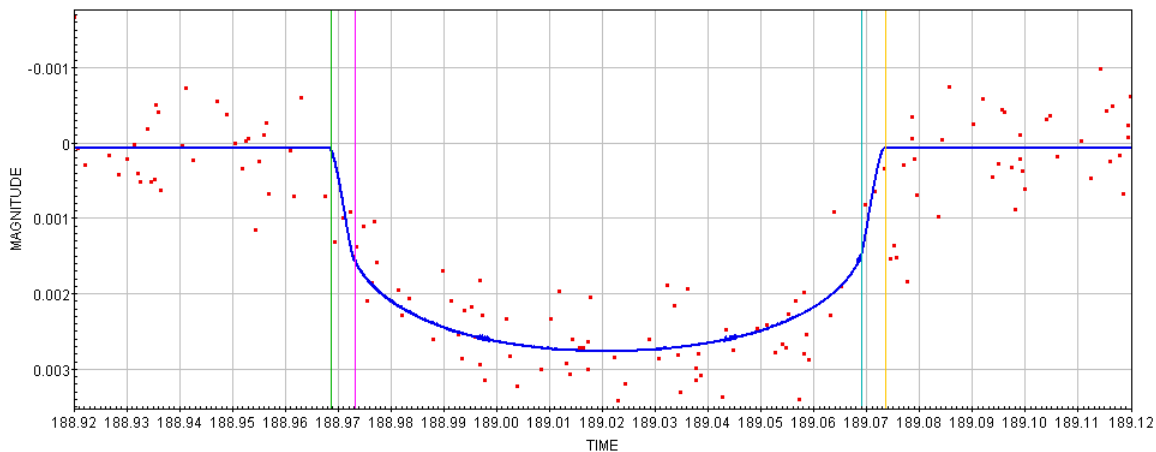


Figure 4.23: Model fit for the Kepler-257 d light curve. Measurements are in long cadence, with 15 transits joined.

The high RMS-to-depth ratio generates large uncertainties on the behavior of the ingress/egress slopes, which are only fitted with poor precision (Figure 4.18). In addition to that, these slopes appear in the model much shorter than what the measured light curve seems to show. Considering that, this fit does not correspond to the measurements and cannot be considered reliable enough to be studied in detail.

4.2.17 Kepler-281 c

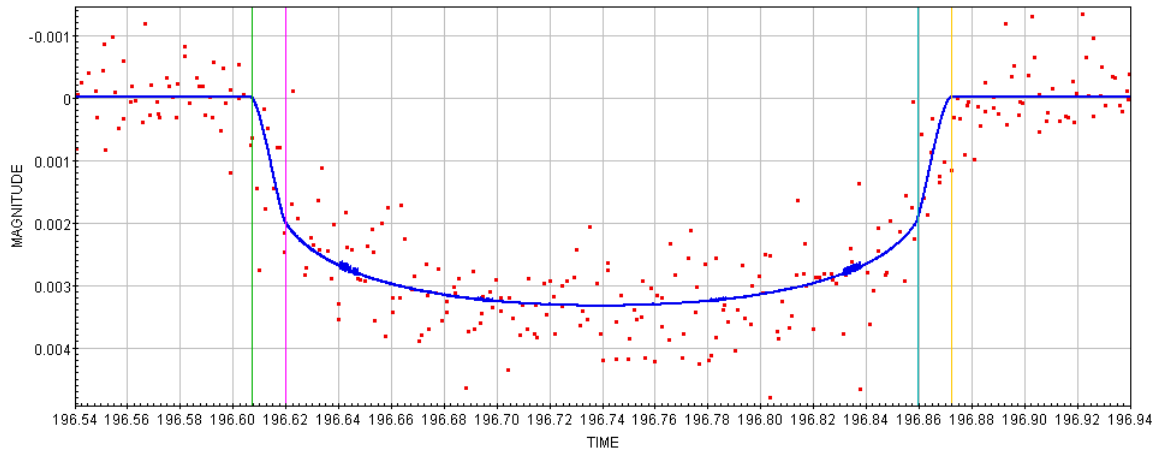


Figure 4.24: Model fit for the Kepler-281 c light curve. Measurements are in long cadence, with 15 transits joined.

Although the light curve of this system presents a relatively large RMS-to-depth ratio, the model fit is in good agreement with the light curve described by the measurements of the flux (Figure 4.15). The characteristic transit times are measured with good precision and well adjusted to the model. The ingress/egress slopes also agree with the measurements, so the reliability of this model is considered good.

4.3 Summary & interpretation of the results

We distribute our measurements and results in 3 different tables, which contain the corresponding parameters of the 18 systems analyzed. One of these systems corresponds to measurements in short cadence, while the other 17 systems correspond to measurements in long cadence. In table 4.2 we show the characteristic transit times measured from the fitting light curves. Table 4.3 shows the parameters associated to the light curve observables, for each system. Finally, table 4.4 contains the stellar parameters we have taken to derive the planetary orbital periods, as well as the results, compared with the real periods. We also computed the estimated periods (Equation 3.9) of the systems associated to poorly fitted light curves, in order to show the importance of having a precise model, to apply the methodology of the unique transit.

We have been mentioning in the previous subsection that transits are supposed to be symmetric. This implies that the ingress and egress slopes ($t_2 - t_1$ & $t_4 - t_3$, respectively) have to be of the same length. We calculated these lengths using the measurements of Table 4.2. We can check that this assumption is perfectly accomplished by looking at Figure 4.25, which proves the reliability assumed for those systems with only one of the ingress/egress slopes properly and precisely defined.

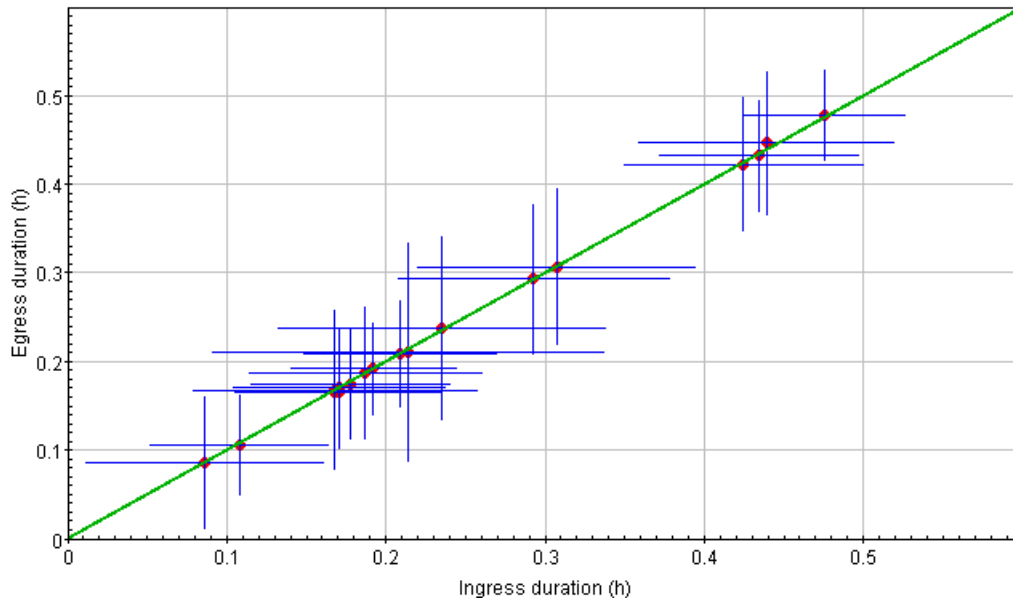


Figure 4.25: Comparison between the ingress and egress lengths of the fitted light curve for the 18 systems analyzed. The red points show the derived lengths, the blue bars represent the uncertainties and the green line shows the expected 1:1 relationship.

Kepler	t_1 (day)	t_2 (day)	t_3 (day)	t_4 (day)	Reliability
18 d	172.6597 ± 0.0015	172.6667 ± 0.0015	172.6974 ± 0.0015	172.7033 ± 0.0015	Poor
26 c	184.3512 ± 0.0022	184.3548 ± 0.0022	184.4252 ± 0.0022	184.4288 ± 0.0022	Poor
27 b	204.6085 ± 0.0019	204.6156 ± 0.0019	204.7475 ± 0.0019	204.7544 ± 0.0019	Good
27 c	184.6592 ± 0.0025	184.6714 ± 0.0025	184.8407 ± 0.0025	184.8529 ± 0.0025	Good
31 b	179.9017 ± 0.0022	179.9095 ± 0.0022	180.0965 ± 0.0022	180.1043 ± 0.0022	Poor
39 b	202.7350 ± 0.0015	202.7548 ± 0.0015	202.9625 ± 0.0015	202.9824 ± 0.0015	Good
89 d	1138.0360 ± 0.0018	1138.0541 ± 0.0018	1138.2951 ± 0.0018	1138.3131 ± 0.0018	Good
117 b	202.0596 ± 0.0024	202.0779 ± 0.0024	202.3451 ± 0.0024	202.3637 ± 0.0024	Good
118 c	201.6606 ± 0.0015	201.6686 ± 0.0015	201.7825 ± 0.0015	201.7905 ± 0.0015	Poor
149 b	185.3354 ± 0.0036	185.3443 ± 0.0036	185.5389 ± 0.0036	185.5477 ± 0.0036	Good
222 d	194.8229 ± 0.0020	194.8300 ± 0.0020	194.9991 ± 0.0020	195.0062 ± 0.0020	Moderate
229 c	173.5479 ± 0.0018	173.5566 ± 0.0018	173.6865 ± 0.0018	173.6952 ± 0.0018	Moderate
230 b	191.9129 ± 0.0026	191.9199 ± 0.0026	192.0941 ± 0.0026	192.1011 ± 0.0026	Moderate
238 e	171.2038 ± 0.0022	171.2215 ± 0.0022	171.5267 ± 0.0022	171.5443 ± 0.0022	Good
247 d	199.1134 ± 0.0030	199.1232 ± 0.0030	199.2218 ± 0.0030	199.2317 ± 0.0030	Poor
248 c	175.4837 ± 0.0018	175.4911 ± 0.0018	175.6461 ± 0.0018	175.6534 ± 0.0018	Good
257 d	188.9686 ± 0.0017	188.9731 ± 0.0017	189.0690 ± 0.0016	189.0734 ± 0.0016	Poor
281 c	196.6071 ± 0.0026	196.6199 ± 0.0026	196.8593 ± 0.0026	196.8721 ± 0.0026	Good

Table 4.2: Characteristic transit times measured and model fit reliability for each system studied.

We have analyzed in detail a total of 18 transiting exoplanets. Their light curves have been fitted very well in 9 of them and moderately well in another 3 systems. On the other hand, there are evident deviations for the remaining 6 systems (Table 4.4).

The estimated periods are at the 1 sigma level with the real periods in 4 of the 6 systems fitted with poor reliability, as their ratios are much smaller than 1 (see Table 4.4), while they are around half the real period for the other 2 systems. These results reflect, again, the necessity of fitting a precise model with transit and flat transit durations properly determined, as it was supposed a priori, since the orbital period depends on their quadratic difference raised to the 3/2 exponent (Equation 5.9). In contrast, the derived periods for the remaining 12 systems are certainly compatible, in general, because 10 of the 12 planets have the real period inside the error margin of the estimated period. The results belonging to these systems are discussed, in a deeper way, next.

There are 2 systems that stand out for not being their derived orbital periods compatible with the real ones, although their fitting models show very good agreement with their measured light curves (Kepler-89 d & Kepler-39 b). We have to remember that we are applying our methodology supposing that all orbits are circular, with zero eccentricity. Otherwise, our method does not work. In the case of Kepler-39 b, the measured eccentricity is $e = 0.121$ ¹, which is not very high, but may be sufficiently far from 0 to significantly alter its orbital motion. Kepler-89 d eccentricity is still unknown, but we can attribute the deviation of its estimated period to a possible non-circular orbit. Another possibility is that the stellar parameters could be erroneous, so they yield an unrealistic result. The other 7 systems for which the reliability of their models are significantly good are highly compatible. Their derived periods are within factors between 0.6 & 1.3 the real periods, and the real periods are found inside the error bars of the calculated periods (Table 4.4).

¹http://exoplanet.eu/catalog/kepler-39_b/

Kepler	N	t_T (h)	t_F (h)	RMS (ppm)	Depth (ppm)	$(t_T^2 - t_F^2)^{3/2}$
18 d	15	3.446 ± 0.050	3.113 ± 0.050	189	2914 ± 571	$3.24^{+1.07}_{-0.96}$
26 c	10	1.862 ± 0.074	1.690 ± 0.074	353	1877 ± 557	$0.48^{+0.50}_{-0.36}$
27 b	15	3.502 ± 0.065	3.166 ± 0.065	526	2836 ± 1089	$3.35^{+1.46}_{-1.27}$
27 c	10	4.649 ± 0.085	4.063 ± 0.085	573	5075 ± 1283	$11.52^{+3.71}_{-3.35}$
31 b	15	4.862 ± 0.073	4.288 ± 0.073	381	1792 ± 500	$6.55^{+2.90}_{-2.52}$
39 b	15	5.938 ± 0.051	4.985 ± 0.051	226	8282 ± 713	$33.57^{+3.85}_{-3.71}$
89 d	30	6.650 ± 0.062	5.784 ± 0.062	486	5164 ± 856	$35.36^{+5.53}_{-5.25}$
117 b	15	7.298 ± 0.080	6.413 ± 0.080	226	2182 ± 463	$42.31^{+8.39}_{-7.87}$
118 c	15	3.118 ± 0.052	2.734 ± 0.052	372	4767 ± 959	$3.37^{+1.01}_{-0.91}$
149 b	6	5.10 ± 0.12	4.67 ± 0.12	238	2087 ± 474	$8.45^{+5.68}_{-4.61}$
222 d	15	4.399 ± 0.066	4.058 ± 0.066	354	1835 ± 632	$4.89^{+2.15}_{-1.87}$
229 c	15	3.535 ± 0.060	3.118 ± 0.060	559	4445 ± 1009	$4.63^{+1.48}_{-1.34}$
230 b	10	4.517 ± 0.089	4.181 ± 0.089	393	1717 ± 616	$5.00^{+3.06}_{-2.53}$
238 e	15	8.172 ± 0.075	7.325 ± 0.075	307	3164 ± 629	$47.57^{+9.17}_{-8.64}$
247 d	10	2.84 ± 0.10	2.37 ± 0.10	590	2628 ± 964	$3.86^{+1.92}_{-1.64}$
248 c	15	4.073 ± 0.062	3.720 ± 0.062	374	2326 ± 674	$4.56^{+1.80}_{-1.59}$
257 d	15	2.515 ± 0.056	2.302 ± 0.056	450	2259 ± 711	$1.04^{+0.63}_{-0.52}$
281 c	15	6.360 ± 0.087	5.746 ± 0.087	465	2767 ± 857	$20.28^{+6.38}_{-5.77}$

Table 4.3: Values of the parameters corresponding to the modeled light curves observables for each system studied. Kepler-89 d has been analyzed using a single transit registered in short cadence, which is equivalent to having joined 30 transits in long cadence, in terms of time sampling.

The 3 systems whose fitted light curves have been considered moderately good have compatible estimation of periods within one sigma of the errors, with period ratios ranging from 0.5 to 0.7. However, their errors are larger than ordinary and this is explained by the large relative uncertainties associated to the stellar radii. Stellar radius is a critical parameter at the time of deriving the orbital period through this method, as it is discussed next, such that these large period uncertainties may be not reliable at all. For these reasons we should question ourselves if the reliability of these 3 models is, indeed, good enough for carrying out our methodology.

Kepler	M_* (M_{Sun})	R_* (R_{Sun})	P (days)	Real P	Ratio	Reliability
18 d	$0.97 \pm 0.04^{1,2}$	$1.11 \pm 0.05^{1,2}$	$3.86^{+1.50}_{-1.19}$	14.86	$0.26^{+0.10}_{-0.08}$	Poor
26 c	$0.63 \pm 0.03^{1,3}$	$0.57 \pm 0.03^{1,3}$	$3.80^{+3.36}_{-2.29}$	17.25	$0.22^{+0.21}_{-0.13}$	Poor
27 b	$0.65 \pm 0.16^{1,2}$	$0.59 \pm 0.15^{1,2}$	$18.09^{+28.04}_{-11.24}$	15.33	$1.18^{+1.83}_{-0.73}$	Good
27 c	$0.65 \pm 0.16^{1,2}$	$0.59 \pm 0.15^{1,2}$	$40.18^{+55.69}_{-23.08}$	31.33	$1.28^{+1.78}_{-0.74}$	Good
31 b	$1.21 \pm 0.09^{1,2}$	1.22 ± 0.24^2	$10.50^{+11.73}_{-5.63}$	20.86	$0.50^{+0.56}_{-0.27}$	Poor
39 b	1.26 ± 0.07^3	1.25 ± 0.07^3	$16.53^{+2.63}_{-2.36}$	21.09	$0.78^{+0.12}_{-0.11}$	Good
89 d	1.28 ± 0.05^2	1.52 ± 0.14^2	$14.02^{+5.61}_{-4.04}$	22.34	$0.63^{+0.25}_{-0.18}$	Good
117 b	$1.13 \pm 0.13^{1,3}$	$1.61 \pm 0.05^{1,3}$	$23.78^{+6.65}_{-5.76}$	18.80	$1.26^{+0.35}_{-0.31}$	Good
118 c	0.77 ± 0.13^3	1.1 ± 0.5^3	$2.22^{+6.86}_{-1.52}$	20.17	$0.11^{+0.34}_{-0.08}$	Poor
149 b	0.91 ± 0.05^3	0.95 ± 0.14^3	$19.24^{+20.69}_{-10.75}$	29.20	$0.66^{+0.71}_{-0.37}$	Good
222 d	0.86 ± 0.05^3	$0.87 \pm 0.38^{1,2}$	$15.10^{+47.23}_{-10.58}$	28.08	$0.54^{+1.68}_{-0.38}$	Moderate
229 c	0.79 ± 0.09^3	$0.73 \pm 0.26^{1,2}$	$11.44^{+23.22}_{-7.07}$	16.07	$0.71^{+1.45}_{-0.44}$	Moderate
230 b	$0.92 \pm 0.05^{1,2}$	0.82 ± 0.41^3	$20.70^{+92.36}_{-15.76}$	32.63	$0.63^{+2.83}_{-0.48}$	Moderate
238 e	1.06 ± 0.15^1	1.43 ± 0.26^1	$27.08^{+22.01}_{-11.89}$	23.65	$1.14^{+0.93}_{-0.50}$	Good
247 d	0.77 ± 0.04^3	0.791 ± 0.106^2	$10.84^{+9.67}_{-5.55}$	20.48	$0.53^{+0.47}_{-0.27}$	Poor
248 c	(0.83)	$0.83 \pm 0.10^{1,2,3}$	$13.09^{+9.45}_{-5.82}$	16.24	$0.81^{+0.58}_{-0.36}$	Good
257 d	0.74 ± 0.14^3	1.0 ± 0.5^3	$1.56^{+6.98}_{-1.19}$	24.66	$0.06^{+0.28}_{-0.05}$	Poor
281 c	0.94 ± 0.09^3	0.9 ± 0.3^3	$45.42^{+85.28}_{-27.81}$	36.34	$1.25^{+2.35}_{-0.77}$	Good

Table 4.4: Summary of derived periods, used parameters and reliability of model fits for each studied system. The mass value in parentheses (Kepler-248 c) is assumed under the approximation $M_* \approx R_*$, since there was no data available. 1: Value taken from NASA Exoplanet Archive. 2: Value taken from The Extrasolar Planet Encyclopedia. 3: Value taken from Open Exoplanet Catalog.

The stellar parameters have a very strong influence on the estimation of orbital planetary periods too, mainly the stellar radius, as the orbital period scales with its inverse cubic power (Equation 5.9). In some cases, the relative uncertainty of the stellar radius is very large (larger than 25%) and this leads to a very large error on the estimated period. This is what happens for the systems Kepler-27 b & c, Kepler-229 c, Kepler-281 c, Kepler-230 b and Kepler-222 d (Table 4.3). It occurs in 3 of the 9 exoplanets with good fit and in the 3 exoplanets having a moderate reliability on their models.

In Figure 4.26 we show the distribution of the computed ratios, between the estimated and the real periods, for the sample of systems studied.

We see that the algorithm applied in JKTEBOP tends to generate fitting light curves with shorter transits and shorter ingress/egress slopes when it fails, which is translated into shorter

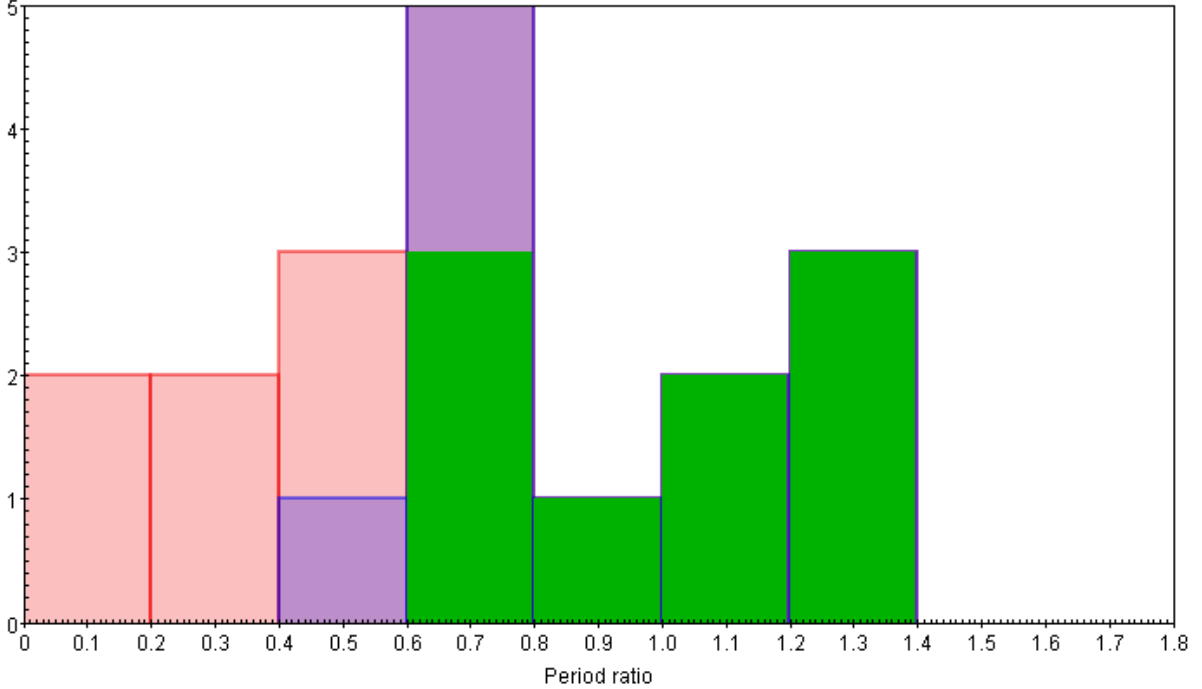


Figure 4.26: Distribution of the ratios between estimated and real periods for the sample of systems analyzed. Green bins correspond to the systems having a high reliable model, blue bins enhance the sample including those systems with moderate reliability and the red bins include the systems removed for having poor fitting models.

periods at the time to apply Equation (5.9), derived by Seager & Mallén-Ornelas (2003). We observe in Figure 4.26 that for systems containing poor fitting models, all of their computed ratios are significantly smaller than 1. Systems whose fitting models are a bit reliable have ratios certainly reduced. Finally, systems properly fitted have computed ratios near unity. Actually, the mean of the ratios for the 9 reliable systems is $1.00^{+1.24}_{-0.51}$, adding those systems with moderate reliability, this mean decreases to $0.91^{+1.51}_{-0.49}$, and including all the systems the mean is $0.70^{+1.24}_{-0.41}$. These errors are significantly large due to the contribution of several large period errors, caused by large uncertainties on the stellar parameters. Neglecting the uncertainties of the stellar masses and radii, these values become $1.00^{+0.28}_{-0.25}$, $0.91^{+0.27}_{-0.24}$ and $0.70^{+0.23}_{-0.21}$, respectively. This seems to show that, in case of a perfect knowledge of the stellar parameters, a sample containing, also, the systems fitted poorly would not agree with the real periods.

Finally, we show plots representing the derived periods, with their errors, as a function of the real periods of all the systems of our sample. We show diagrams for all the systems (Figure 4.27) and another excluding the 6 systems poorly fitted (Figure 4.28).

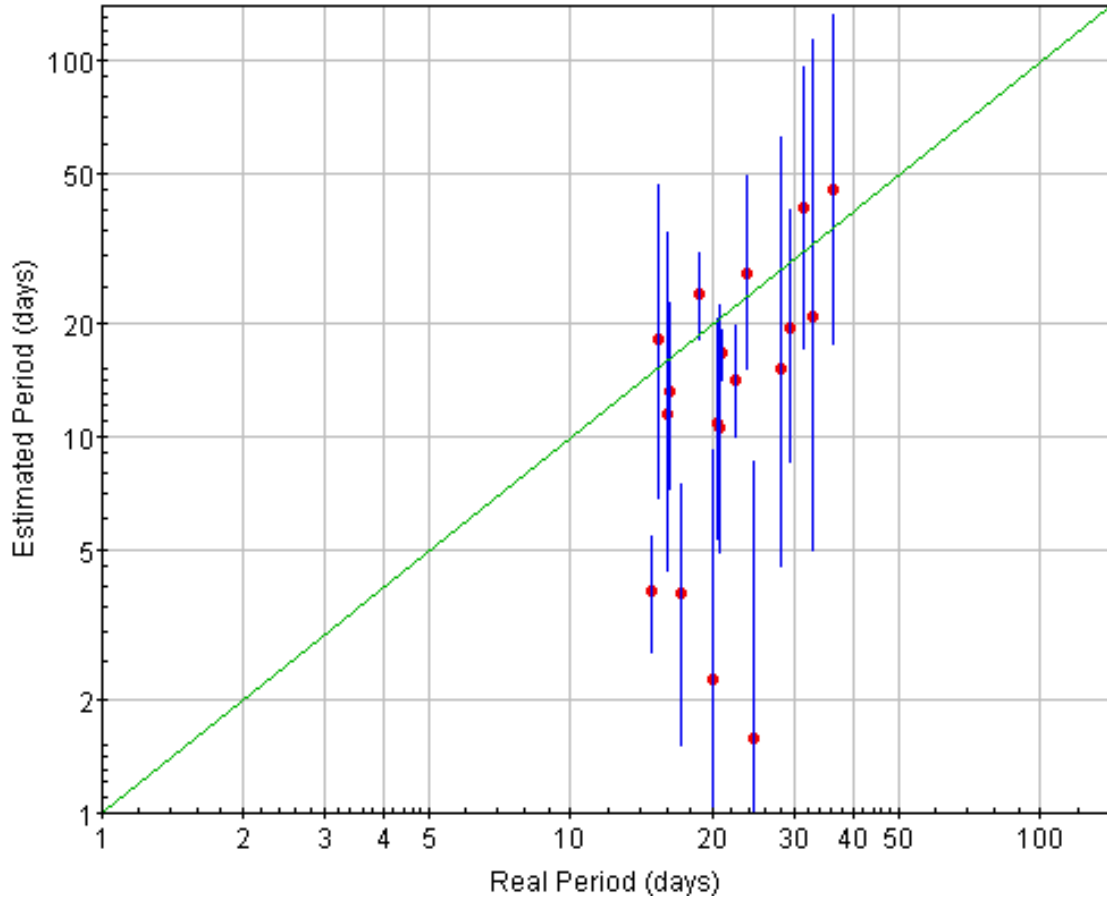


Figure 4.27: Derived periods for each system in function of their real periods. Red points represent the measurements, blue bars show the errors of the estimated periods and the green line represent the 1:1 relationship.

One more time, the evidence of needing a good-fitting model is reflected in Figures 4.27 & 4.28, in the same way as in Table 4.3. We observe 6 of the 18 systems whose real period is not found inside the error margin of the estimated period (Figure 4.27), whereas removing the systems fitted poorly, the number of real periods found out of the errors decreases to 2 of 12 (Figure 4.28). In other words, 4 of the 6 real periods found outside the error ranges correspond to systems without a reliable fitting model.

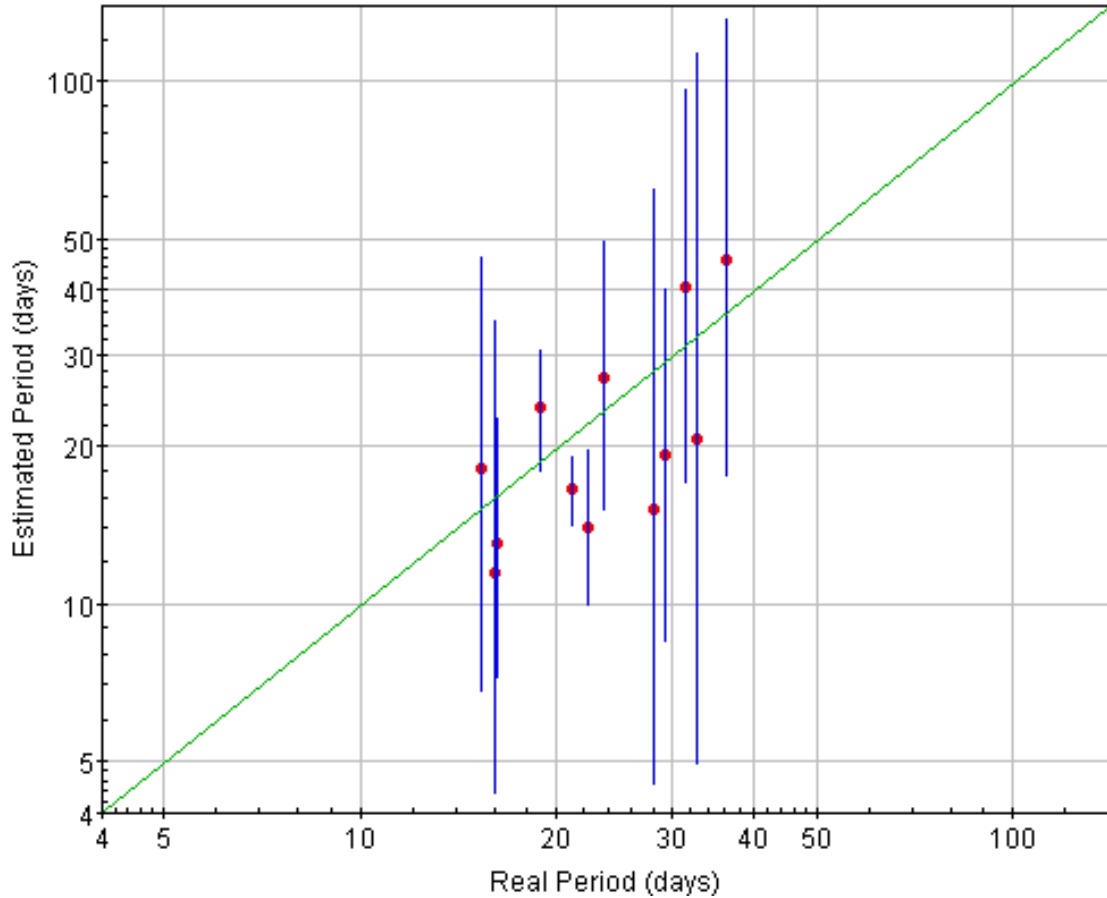


Figure 4.28: Derived periods, removing the systems without reliable fitting model, in function of their real periods. Red points represent the measurements, blue bars show the errors of the estimated periods and the green line represent the 1:1 relationship.

We can also observe the high contribution of the stellar radius error to the derived period error. We provide, in Table 4.5, a comparison of the errors obtained with the errors that we would obtain assuming that the stellar densities (masses and radii) were perfectly known. The hypothetical values assumed are the central values shown in Table 4.4.

Kepler	P (days)	no SP errors	Ratio	no SP errors	Reliability
18 d	$3.86^{+1.50}_{-1.19}$	$3.86^{+0.99}_{-0.91}$	$0.26^{+0.10}_{-0.08}$	$0.26^{+0.07}_{-0.06}$	Poor
26 c	$3.80^{+3.36}_{-2.29}$	$3.80^{+2.86}_{-2.12}$	$0.22^{+0.21}_{-0.13}$	$0.22^{+0.17}_{-0.12}$	Poor
27 b	$18.09^{+28.04}_{-11.24}$	$18.09^{+6.66}_{-6.08}$	$1.18^{+1.83}_{-0.73}$	$1.18^{+0.43}_{-0.40}$	Good
27 c	$40.18^{+55.69}_{-23.08}$	$40.18^{+10.62}_{-9.86}$	$1.28^{+1.78}_{-0.74}$	$1.28^{+0.33}_{-0.31}$	Good
31 b	$10.50^{+11.73}_{-5.63}$	$10.50^{+3.64}_{-3.26}$	$0.50^{+0.56}_{-0.27}$	$0.50^{+0.17}_{-0.16}$	Poor
39 b	$16.53^{+2.63}_{-2.36}$	$16.53^{+1.54}_{-1.50}$	$0.78^{+0.12}_{-0.11}$	$0.78^{+0.07}_{-0.07}$	Good
89 d	$14.02^{+5.61}_{-4.04}$	$14.02^{+1.98}_{-1.92}$	$0.63^{+0.25}_{-0.18}$	$0.63^{+0.09}_{-0.09}$	Good
117 b	$23.78^{+6.65}_{-5.76}$	$23.78^{+4.28}_{-4.12}$	$1.26^{+0.35}_{-0.31}$	$1.26^{+0.23}_{-0.22}$	Good
118 c	$2.22^{+6.86}_{-1.52}$	$2.22^{+0.53}_{-0.49}$	$0.11^{+0.34}_{-0.08}$	$0.11^{+0.03}_{-0.02}$	Poor
149 b	$19.24^{+20.69}_{-10.75}$	$19.24^{+9.43}_{-7.77}$	$0.66^{+0.71}_{-0.37}$	$0.66^{+0.32}_{-0.27}$	Good
222 d	$15.10^{+47.23}_{-10.58}$	$15.10^{+5.44}_{-4.93}$	$0.54^{+1.68}_{-0.38}$	$0.54^{+0.19}_{-0.18}$	Moderate
229 c	$11.44^{+23.22}_{-7.07}$	$11.44^{+2.93}_{-2.71}$	$0.71^{+1.45}_{-0.44}$	$0.71^{+0.18}_{-0.17}$	Moderate
230 b	$20.70^{+92.36}_{-15.76}$	$20.70^{+9.81}_{-8.40}$	$0.63^{+2.83}_{-0.48}$	$0.63^{+0.30}_{-0.26}$	Moderate
238 e	$27.08^{+22.01}_{-11.89}$	$27.08^{+4.68}_{-4.50}$	$1.14^{+0.93}_{-0.50}$	$1.14^{+0.20}_{-0.19}$	Good
247 d	$10.84^{+9.67}_{-5.55}$	$10.84^{+4.35}_{-3.88}$	$0.53^{+0.47}_{-0.27}$	$0.53^{+0.21}_{-0.19}$	Poor
248 c	$13.09^{+9.45}_{-5.82}$	$13.09^{+4.17}_{-3.80}$	$0.81^{+0.58}_{-0.36}$	$0.81^{+0.26}_{-0.23}$	Good
257 d	$1.56^{+6.98}_{-1.19}$	$1.56^{+0.72}_{-0.61}$	$0.06^{+0.28}_{-0.05}$	$0.06^{+0.03}_{-0.02}$	Poor
281 c	$45.42^{+85.28}_{-27.81}$	$45.42^{+12.56}_{-11.80}$	$1.25^{+2.35}_{-0.77}$	$1.25^{+0.35}_{-0.32}$	Good

Table 4.5: Comparison of period and ratio errors with errors obtained assuming perfect knowledge of the stellar density.

The errors of the estimated orbital periods could be much smaller in the ideal case that we knew exactly the stellar parameters (SP). We can observe in Table 4.5 that none of the calculated periods for the systems, whose model fit reliability is poor or moderate, would agree with their real periods. Furthermore, the agreement would be good, only for 5 of the 9 systems with good fit. However, this does not mean that most of our fits are poor. We should note that the SP, assumed to be the exact ones, may be erroneous, since they are really known with a certain error (Table 4.4), and the real values might be different from the central values of SP determined to date.

5 Conclusions

In this master thesis we have tested the reliability of the methodology described by Seager & Mallén-Ornelas (2003) to estimate orbital planetary periods using a single transit, applying their derived analytical equation. The goal of that is to check if for many of the future single transits, expected to be detected by the TESS telescope, will be worth applying the technique of the single transit to them, in order to determine some of the key parameters of those exoplanet candidates and then decide to perform follow-up observations with CHEOPS telescope, since we will be supposed to know what time to observe. We have taken the real periods of those systems studied, in order to compare our own results, from Kepler Mission data. We selected a preliminary sample of 22 exoplanets, 18 of them which have been analyzed deeply.

Large random noise on the measurements of the flux prevents a reliable fit of the light curves, unless transits are very deep. Actually, only one system (Kepler-89 d) has been properly fitted when we have worked with short cadence data, as its transit is quite deep and RMS is relatively small. In contrast, only 1 of the 21 systems, analyzed with long cadence (lower noise), is discarded because of its measured noise.

Although working with long cadence (30 minutes) we do not have as many problems with noise as in short cadence (1 minute), we have had to join several transits inside one, as we needed several points inside the ingress/egress transit slopes, in order to define them with precision. The technique of folding several transits is not applicable when exoplanets have transit timing variations (Kepler-46 b, Kepler-9 b & Kepler-9 c, and in a weaker way some other systems), which makes to appear errors in transit times, obligating us to remove these systems from our analysis. After that, we kept a sample of 18 exoplanets, 1 analyzed at short cadence and the rest, at long cadence.

From our final sample of 18 exoplanets, their light curves have been well fitted for 9 systems and certainly well for other 3 systems, whereas the deviations in the rest of systems are explained as they present TTVs (Kepler-247 d & Kepler-26 c) or the random noise causes deviations on the slopes of the model light curve and duration of ingress/egress periods (Kepler-118 c, Kepler-18 d, Kepler-257 d and Kepler-31 b). In contrast, for all the light curves properly fitted, the estimated period is usually close to the real period, being the estimated period between half and twice the real period in all cases. For these reasons, we conclude that the methodology works well, as long as we are able to give fitting models with sufficient precision, and the planets describe nearly circular orbits.

Because TESS will look for transits in nearer and brighter stars than Kepler stars and TESS will measure fluxes with the same cadence as Kepler, we would expect to obtain light curves

in short cadence with better precision than those obtained by Kepler. Thus, TESS should gather a quite extensive sample of candidates, being their light curves able to be properly fitted. Nevertheless, this method presents the drawback that as the transit depth decreases, the precision of the fitting models also decreases, probably making that the method of the single transit works only in a few cases for Earth-like candidates.

We also need to mention that most of errors that are very large, in systems fitted by reliable models, are caused by large errors in measured stellar radius, and this means that stellar parameters need to be known with enough precision, since we have seen that a small variation on the stellar radius may cause an important change in the derived period. This is critical if we want to consider the possibility of performing follow-up observations of those interesting transits found by TESS with the CHEOPS telescope. Unless the periods are estimated with very good precision and low error, many of the transits will have been lost at the time to study them with CHEOPS. A requisite to derive the orbital period by the single transit method is to previously determine the stellar density (mass and radius) with very low error. It is expected to obtain good measurements of the stellar parameters with Gaia mission (Eyer et al. 2013) and from measurements performed with asteroseismology.

To sum up, as general conclusions we say that the analytical expression used works well but requires previous accurate knowledge of the density of the central star. Also, in order to obtain good fits for each light curve, it is needed to measure the fluxes with a high precision and a short enough cadence, so that we can resolve the ingress/egress parts of the transit, and determine with precision the transit times of contact.

In case of being the CHEOPS-TESS synergy successful, the sample of exoplanets discovered by the next transit survey generation could be enhanced, including not only close-in exoplanets, but also planets with longer orbital periods located in the habitable zones of a large range of stars. This should be relevant since just a handful of this type of planets have been found so far. Furthermore, it is also interesting to discover planets located far from their stars since few systems are known, in order to study and compare the characteristics of other planetary systems with our Solar system.

6 References

Borucki, W., et al. 2009, *IAU*, 253, 289

Broeg, C., et al. 2013, *EPJWC*, 47, 03005

Burke, C., J., et al. 2015, *ApJ*, 809, 8

Eyer, L., et al. 2013, *CEAB*, 37, 115

Fischer, D., A., et al. 2014, *Protostars and Planets*, 914, 715

Fressin, F., et al. 2013, *ApJ*, 766, 81

Jenkins, J., M., et al. 2015, *AJ*, 150, 56

Kipping, D., M., 2013, *Monthly Notices of the Royal Astronomical Society*, 435, 2152

Ricker, G., R., et al. 2014, *JATIS*

Seager, S.; Mallén-Ornelas, G. 2003, *AJ*, 585, 1038

Sing, D., K., 2010, *A&A*, 510, 21

Southworth, J., 2012, *Astrophysics Source Code Library*, 1207.013

Sullavin, P., W., et al. 2015, *ApJ*, 809, 77

7 Appendix

Kepler	Radii sum	Radii ratio	Orb. Inclination (°)	TML (day)	LD lin.	LD non-lin.
18 d	0.031	0.052	89.95	172.733	0.48	0.21
26 c	0.024	0.049	88.81	184.39	0.5	0.22
27 b	0.031	0.052	89.95	204.684	0.48	0.2
27 c	0.032	0.077	88.81	184.76	0.48	0.2
31 b	0.032	0.042	89.95	180.01	0.29	0.32
39 b	0.037	0.089	89.95	202.86	0.32	0.3
89 d	0.039	0.069	89.95	1138.174	0.34	0.29
117 b	0.056	0.047	88.81	202.21	0.29	0.31
118 c	0.020	0.067	89.95	201.725	0.5	0.19
149 b	0.023	0.042	89.95	185.445	0.44	0.23
222 d	0.022	0.041	89.38	194.918	0.45	0.22
229 c	0.029	0.065	89.95	173.624	0.52	0.17
230 b	0.013	0.043	89.95	292.011	0.44	0.23
238 e	0.045	0.054	89.95	171.372	0.38	0.27
247 d	0.039	0.058	88.24	199.183	0.53	0.17
248 c	0.033	0.046	89.95	175.57	0.52	0.17
257 d	0.025	0.053	88.81	189.025	0.51	0.18
281 c	0.040	0.056	88.24	196.74	0.4	0.25

Table 7.1: Input parameters introduced in JKTEBOP to obtain the light curve fits for each system.